J|A|C|S
ARTICLES

Published on Web 03/01/2010

A Chiral Wedge Molecule Inhibits Telomerase Activity

Ken-ichi Shinohara,[†] Yuta Sannohe,[†] Shuji Kaieda,[†] Ken-ichi Tanaka,[‡] Hideji Osuga,[‡] Hidetoshi Tahara,[§] Yan Xu,[†,⊥] Takashi Kawase,[†] Toshikazu Bando,[†] and Hiroshi Sugiyama*[,†,∥]

Department of Chemistry, Graduate School of Science, Kyoto University, Sakyo-ku Kyoto 606-8502, Japan, Department of Materials Science and Chemistry, Faculty of Systems Engineering, Wakayama University, 930 Sakaedani Wakayama 640-8510, Japan, Department of Cellular and Molecular Biology, Hiroshima University, Hiroshima 734-8553, Japan, Research Center for Advanced Science and Technology, The University of Tokyo, 4-6-1 Komaba Meguro-ku Tokyo 153-8904, Japan, and Institute for Integrated Cell-Material Sciences (iCeMS), Kyoto University, Sakyo-ku Kyoto 606-8501, Japan

Received October 19, 2009; E-mail: hs@kuchem.kyoto-u.ac.jp

Abstract: In addition to the Watson−Crick double helix, secondary DNA structures are thought to play important roles in a variety of biological processes. One important example is the G-quadruplex structure that is formed at the chromosome ends, which inhibits telomerase activity by blocking its access to telomeres. G-quadruplex structures represent a new class of molecular targets for DNA-interactive compounds that may be useful to target telomeres. Here, we reported the first example of enantioselective recognition of quadruplex DNA by a chiral cyclic helicene. We propose a new ligand-binding cleft between two telomeric human G-quadruplexes linked by a TTA linker. We found that the cyclic helicene M1 exhibited potent inhibitory activity against telomerase.

Introduction

Human telomeres, which are nucleoprotein complexes present at chromosome ends, consist of tandem arrays of TTAGGG repeats that can be elongated by adding single repeat units.[1−3] Telomerase is an important enzyme that is involved in telomere maintenance.[4,5] The enzyme is activated in 80−90% of human tumors and is low or undetectable in most normal somatic cells.[6] Thus, telomerase represents a target with good selectivity for tumorous over healthy tissues, and telomerase inhibition has been identified as a new approach to cancer therapy.[7−18] Folding of telomeric DNA into four-strand G-quadruplexes inhibits telomerase by locking the single-stranded telomeric substrate into an inactive conformation that is no longer recognized, nor elongated, by the enzyme.[19] Such quadruplexes are potential tumor-selective targets for chemotherapy.[19−22] Several quadruplex-specific ligands reportedly interact with quadruplexes and act as inhibitors of telomerase activity;[23−28] these include

[†] Graduate School of Science, Kyoto University.
[‡] Wakayama University.
[§] Hiroshima University.
[⊥] The University of Tokyo.
[∥] iCeMS, Kyoto University.

(1) Blackburn, E. H. *Cell* **1994**, *77*, 621−623.
(2) Zakian, V. A. *Science* **1995**, *270*, 1601−1607.
(3) Greider, C. W. *Annu. Rev. Biochem.* **1996**, *65*, 337−365.
(4) McEachern, M. J.; Krauskopf, A.; Blackburn, E. H. *Annu. Rev. Genet.* **2000**, *34*, 331−358.
(5) Kim, N. W.; Piatyszek, M. A.; Prowse, K. R.; Harley, C. B.; West, M. D.; Ho, P. L.; Coviello, G. M.; Wright, W. E.; Weinrich, S. L.; Shay, J. W. *Science* **1994**, *266*, 2011−2015.
(6) Raymond, E.; Sun, D.; Chen, S. F.; Windle, B.; Von Hoff, D. D. *Curr. Opin. Biotechnol.* **1996**, *7*, 583−591.
(7) Hahn, W. C.; Stewart, S. A.; Brooks, M. W.; York, S. G.; Eaton, E.; Kurachi, A.; Beijersbergen, R. L.; Knoll, J. H.; Meyerson, M.; Weinberg, R. A. *Nat. Med.* **1999**, *5*, 1164−1170.
(8) Cech, T. R. *Angew. Chem., Int. Ed.* **2000**, *39*, 34−43.
(9) Shay, J. W.; Zou, Y.; Hiyama, E.; Wright, W. E. *Hum. Mol. Genet.* **2001**, *10*, 677−685.
(10) Rezler, E. M.; Bearss, D. J.; Hurley, L. H. *Curr. Opin. Pharmacol.* **2002**, *2*, 415−423.
(11) Mergny, J. L.; Riou, J. F.; Mailliet, P.; Teulade-Fichou, M. P.; Gilson, E. *Nucleic Acids Res.* **2002**, *30*, 839−865.
(12) Cairns, D.; Anderson, R. J.; Perry, P. J.; Jenkins, T. C. *Curr. Pharm. Des.* **2002**, *8*, 2491−2504.
(13) Huard, S.; Autexier, C. *Curr. Med. Chem. Anticancer Agents* **2002**, *2*, 577−587.
(14) Rezler, E. M.; Bearss, D. J.; Hurley, L. H. *Annu. Rev. Pharmacol. Toxicol.* **2003**, *43*, 359−379.
(15) Kelland, L. R. *Eur. J. Cancer* **2005**, *41*, 971−979.
(16) Shay, J. W.; Wright, W. E. *Nat. Rev. Drug Discovery* **2006**, *5*, 577−584.
(17) Pendino, F.; Tarkanyi, I.; Dudognon, C.; Hillion, J.; Lanotte, M.; Aradi, J.; Segal-Bendirdjian, E. *Curr. Cancer Drug Targets* **2006**, *6*, 147−180.
(18) Cian, A. D.; Lacroix, L.; Douarre, C.; Smaali, N. T.; Trentesaux, C.; Riou, J.; Mergny, J. L. *Biochimie* **2008**, *90*, 131−155.
(19) Zahler, A. M.; Williamson, J. R.; Cech, T. R.; Prescott, D. M. *Nature* **1991**, *350*, 718−720.
(20) Neidle, S.; Parkinson, G. N. *Nat. Rev. Drug Discovery* **2002**, *1*, 383−393.
(21) Chen, B.; Liang, J.; Tian, X.; Liu, X. *Biochemistry (Moscow)* **2007**, *73*, 853−861.
(22) Oganesian, L.; Bryan, T. M. *BioEssays* **2007**, *29*, 155−165.
(23) Read, M.; Harrison, R. J.; Romagnoli, B.; Tanious, F. A.; Gowan, S. H.; Reszka, A. P.; Wilson, W. D.; Kelland, L. R.; Neidle, S. *Proc. Natl. Acad. Sci. U.S.A.* **2001**, *98*, 4844−4849.
(24) Riou, J. F.; Guittat, L.; Mailliet, P.; Laoui, A.; Renou, E.; Petitgenet, O.; Megnin-Chanet, F.; Helene, C.; Mergny, J. L. *Proc. Natl. Acad. Sci. U.S.A.* **2002**, *99*, 2627−2677.
(25) Teulade-Fichou, M. P.; Carrasco, C.; Guittat, L.; Bailly, C.; Alberti, P.; Mergny, J. L.; David, A.; Lehn, J. M.; Wilson, W. D. *J. Am. Chem. Soc.* **2003**, *125*, 4732−4740.
(26) Jantos, K.; Rodriguez, R.; Ladame, S.; Shirude, P. S.; Balasubramanian, S. *J. Am. Chem. Soc.* **2006**, *128*, 13662−13663.

10.1021/ja908897j

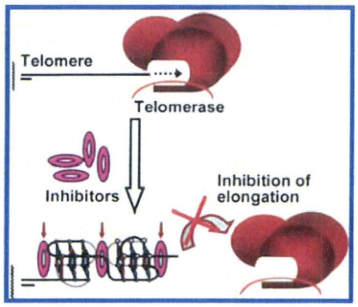

Figure 1. Schematic representation of telomerase inhibition by the G-quadruplex structure formed at the end of human chromosomes, which is stabilized by the binding of the ligand to the cleft pocket formed by the quadruplex dimer.

acridine derivatives, cationic porphyrin derivatives, and telomestatin.[29−33] Crystallographic, NMR, and computer modeling studies were performed to obtain detailed information on quadruplex structures and on the interaction of quadruplex DNA with, and stabilization by, small molecules.[34−38] Single quadruplex units (which are typically human telomeric sequences of 22 nt) were used as target structures in most of these previous studies. However, taking into account the length of the 3′-terminal single-stranded human telomeric DNA (100−200 bases),[39−41] a higher-order G-quadruplex structure would be formed in this region to inhibit telomerase activity (Figure 1a). Two groups proposed that two individual quadruplex structures could form a quadruplex dimer.[42,43] Recently, ours and two other groups demonstrated the formation of mixed parallel/antiparallel human telomeric G-quadruplexes with unique topology in K^+ solutions, suggesting the possibility of clustering of the 22 nt sequence units into higher-order packed structures.[44−49] However, it remains unclear how the ligands of G-quadruplex structures bind to telomeres in living cells (which contain a large amount of TTAGGG repeats) and lead to telomerase inhibition. We predict that the cleft pocket located between two telomeric human G-quadruplexes is formed in living cells when the G-quadruplexes are stabilized by the binding of the ligand (Figure 1a). Therefore, it would be important to use DNA molecules that are longer than 22 nt for the evaluation of G-quadruplex ligands. Recently, atomic force microscopy (AFM) observation of long telomeric DNA revealed the existence of consecutive G-quadruplex structures.[50] These superhelical structures may be suitable for ligand binding, which inhibits telomerase activity.

Here, we reported a cyclic helicene molecule that displayed chiral and steric selection during binding to quadruplex superhelical structures and exhibited potent inhibitory activity against telomerase. We reported previously that the simple helicene molecule (M)-A (Figure 2a) discriminates between B- and Z-DNA, binds to Z-DNA, and stabilizes Z-DNA conformation enantioselectively.[51] As the cleft pockets between G-quadruplex units should involve chiral-rich spaces and Z-DNA, here we investigated whether chiral helicene molecules had the ability to bind to the cleft pocket and stabilize G-quadruplex structures enantioselectively.

Results and Discussion

The newly targeted substrate ODN 1 (AGGG(TTAGGG)$_3$TTAGGG(TTAGGG)$_3$) used in this study consisted of a quadruplex dimer formed by two G-quadruplex repeats stacked 3′ to 5′ with a TTA linker. The ODN 2 substrate (AGGG(TTAGGG)$_3$(TTA)$_6$GGG(TTAGGG)$_3$), which contained six TTA repeats and in which the G-quadruplexes were divided into two separate units by the longer TTA repeated sequence, was used as a control. We first examined the binding of (P)-A and (M)-A to ODN 1 (Figure 2a). Both helicenes bound to ODN 1 but did not show enantioselectivity (Supporting Information Figure S1). We assumed that the dihedral angle of the helicene might contribute to the interaction; therefore, a series of chiral cyclic helicene molecules were prepared (Figure 2b). X-ray analysis indicated that the dihedral angle of the helical framework varied significantly from 22 to 59°, which suggests that the planarity of the helicenes decreased with the increasing length of the linker bridge.[52] The binding behavior of the helicenes to ODN 1 was examined using circular dichroism (CD) spectroscopy, which revealed an apparent 70% decrease in CD intensity during the binding of M1 to ODN 1, whereas no marked changes occurred during the binding of the other helicenes to ODN 1 (Figure 3a−c). To elucidate the molecular basis of the interaction of the helicene with the TTAGGG

(27) Brassart, B.; Gomez, D.; Cian, A. D.; Paterski, R.; Montagnac, A.; Qui, K. H.; Smaali, N. T.; Trentesaux, C.; Mergney, J. L.; Gueritte, F.; Riou, J. F. *Mol. Pharmacol.* **2007**, *72*, 631–640.
(28) Yu, H.; Wang, X.; Fu, M.; Ren, J.; Qu, X. *Nucleic Acids Res.* **2008**, *36*, 5695–5703.
(29) Koeppel, F.; Riou, J. F.; Laoui, A.; Mailliet, P.; Arimondo, P. B.; Labit, D.; Petitgenet, O.; Helene, C.; Mergny, J. L. *Nucleic Acids Res.* **2001**, *29*, 1087–1096.
(30) Han, H.; Langley, D. R.; Rangan, A.; Hurley, L. H. *J. Am. Chem. Soc.* **2001**, *123*, 8902–8913.
(31) Shin-ya, K.; Wierzba, K.; Matsuo, K.; Ohtani, T.; Yamada, Y.; Furihata, K.; Hayakawa, Y.; Seto, H. *J. Am. Chem. Soc.* **2001**, *123*, 1262–1263.
(32) Reed, J. E.; Arnal, A. A.; Neidle, S.; Vilar, R. *J. Am. Chem. Soc.* **2006**, *128*, 5992–5993.
(33) Baker, E. S.; Lee, J. T.; Sessler, J. L.; Bowers, M. T. *J. Am. Chem. Soc.* **2006**, *128*, 2641–2648.
(34) Clark, G. R.; Pytel, P. D.; Squire, C. J.; Neidle, S. *J. Am. Chem. Soc.* **2003**, *125*, 4066–4067.
(35) Gavathiotis, E.; Heald, R. A.; Stevens, M. F. G.; Searle, M. S. *J. Mol. Biol.* **2003**, *334*, 25–36.
(36) Parkinson, G. N.; Ghosh, R.; Neidle, S. *Biochemistry* **2007**, *46*, 2390–2397.
(37) Campbell, N. H.; Parkinson, G. N.; Reszka, Ap.; Neidle, S. *J. Am. Chem. Soc.* **2008**, *130*, 6722–6724.
(38) Parkinson, G. N.; Cuenca, F.; Neidle, S. *J. Mol. Biol.* **2008**, *381*, 1145–1156.
(39) Makarov, V. L.; Hirose, Y.; Langmore, J. P. *Cell* **1999**, *88*, 657–666.
(40) McElligott, R.; Wellinger, R. J. *EMBO J.* **1997**, *16*, 3705–3714.
(41) Wright, W. E.; Tesmer, V. M.; Huffman, K. E.; Levene, S. D.; Shay, J. W. *Genes Dev.* **1997**, *11*, 2801–2809.
(42) Haider, S.; Parkinson, G. N.; Neidle, S. *Biophys. J.* **2008**, *95*, 296–311.
(43) Petraccone, L.; Trent, J. O.; Chaires, J. B. *J. Am. Chem. Soc.* **2008**, *130*, 16530–16532.
(44) Xu, Y.; Noguchi, Y.; Sugiyama, H. *Bioorg. Med. Chem.* **2006**, *14*, 5584–5591.
(45) Ambrus, A.; Chen, D.; Dai, J.; Bialis, T.; Jones, R. A.; Yang, D. *Nucleic Acids Res.* **2006**, *34*, 2723–2735.
(46) Luu, K. N.; Phan, A. T.; Kuryavyi, V.; Lacroix, L.; Patel, D. J. *J. Am. Chem. Soc.* **2006**, *128*, 9963–9970.
(47) Matsugami, A.; Xu, Y.; Noguchi, Y.; Sugiyama, H.; Katahira, M. *FEBS J.* **2007**, *274*, 3545–3556.
(48) Phan, A. T.; Kuryavyi, V.; Luu, K. N.; Patel, D. J. *Nucleic Acids Res.* **2007**, *35*, 6517–6525.
(49) Dai, J.; Carver, M.; Punchihewa, C.; Jones, R. A.; Yang, D. *Nucleic Acids Res.* **2007**, *35*, 4927–4940.
(50) Xu, Y.; Ishizuka, T.; Kurabayashi, K.; Komiyama, M. *Angew. Chem., Int. Ed.* **2009**, *48*, 3281–3284.
(51) Xu, Y.; Zhang, Y. X.; Sugiyama, H.; Umano, T.; Osuga, H.; Tanaka, K. *J. Am. Chem. Soc.* **2004**, *126*, 6566–6567.
(52) Tanaka, K.; Osuga, H.; Kitahara, Y. *J. Org. Chem.* **2002**, *67*, 1795–1801.

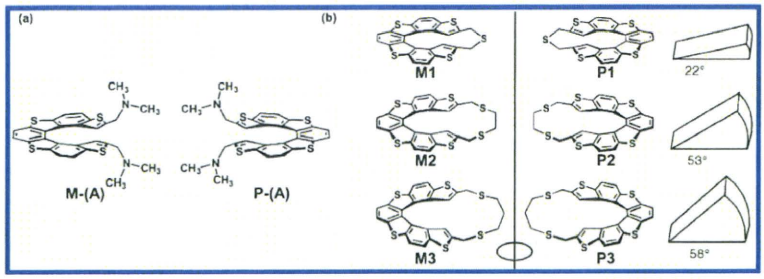

Figure 2. (a) Structures of the helicenes (M)-A and (P)-A, which bind enantioselectively to Z-DNA and B-DNA, respectively.[51] (b) Structures of the cyclic helicenes that were examined as higher-order G-quadruplex ligands. The dihedral angle of the helical frameworks increased from 22 to 58°.[52]

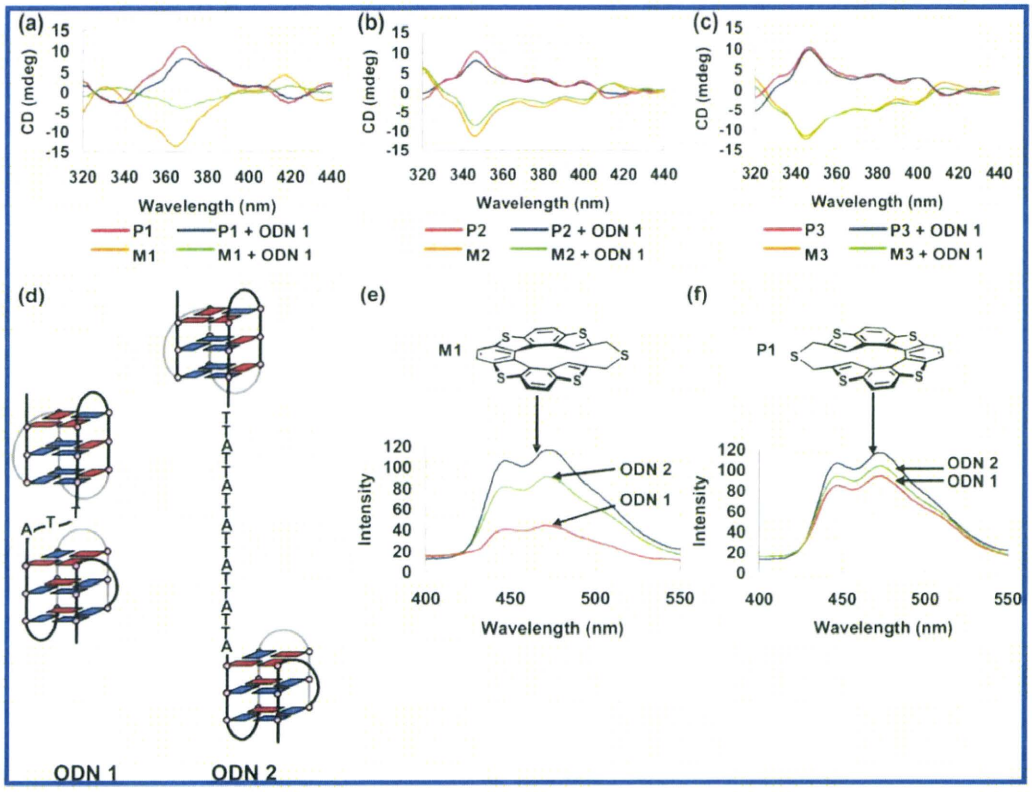

Figure 3. (a–c) CD spectra of the M1–M3 and P1–P3 helicenes (3 μM, 25 °C) in the presence or absence of ODN 1 (1.5 μM strand concentration) in 2 mM K-cacodylate buffer (pH 7.0) and in the presence of 150 mM KCl. (d) Targeted substrates used in the study; ODN 1 with a TTA linker formed a higher-order quadruplex dimer; ODN 2 with six TTA repeats was used as a control, as the longer bridge linker divided the G-quadruplexes into two separate units. (e,f) Fluorescence spectra (excitation at 330 nm) of (a) M1 and (b) P1 (1.0 μM, 25 °C) in 2 mM K-cacodylate buffer (pH 7.0), in the presence or absence of ODN 1 and ODN 2 in 100 mM KCl.

repeats, fluorescence measurements using ODN 2 were performed in parallel experiments. Strong quenching (80%) of the fluorescence of M1 was observed in the presence of ODN 1 compared with ODN 2 (Figure 3e). Conversely, P1 did not lead to a significant change in fluorescence after binding to ODN 1 or ODN 2 under the same conditions (Figure 3f). These results suggest that M1 binds preferentially to the dimer quadruplex ODN 1 in an enantioselective manner. The binding constants of helicene to DNA were examined using surface plasmon resonance (SPR) with biotinylated telomeric DNA. The observed SPR sensorgrams are shown in Figure 4. M1 exhibited a significant response curve at micromolar concentrations, whereas a response curve was not observed for P1, even at the concentration of 1 mM. The dissociation constants of M1 for ODN 1 and ODN 2 were estimated at 433(±13) and 475(±8) nM, respectively. Moreover, we investigated the binding of M1 to ODN 3, which contained four simple TTAGGG repeats (Supporting Information Figure S2). We observed an efficient reduction of fluorescence and a decrease in CD intensity in the presence of M1 and ODN 1, as shown in Figure 3, whereas there was no significant difference regarding the dissociation constants of M1 for ODN 1–3, as assessed using an SPR

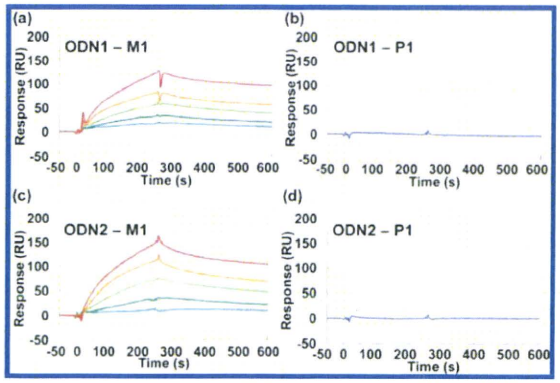

Figure 4. (a–d) SPR sensorgrams of the interaction of M1 and P1 with ODN 1 and ODN 2 in HEPES buffer (pH 7.4) in the presence of 200 mM KCl. The concentration of M1 ranged from 0.25 to 4 μM, and the concentration of P1 was 1 mM.

Table 1. Dissociation Constants of Helicene from DNA Determined Using the SPR Method (ODN 3 Contained Four Telomere Repeats)

	M1	P1
ODN 1	433 ± 13 nM	not determined
ODN 2	475 ± 8 nM	not determined
ODN 3	541 ± 11 nM	not determined

approach (Table 1). This discrepancy may be due to differences in the sensitivity of the methods or to the optical characteristic of the compounds. However, it is important to consider that P1 never bound to TTAGGG repeats. These results confirmed that M1 binds enantioselectively to quadruplex DNA.

Further analysis aimed at establishing the enantioselectivity of M1 and P1 was performed using the modified telomeric repeat amplification protocol (TRAP) assay—"stretch PCR".[53–55] In the presence of the M1 helicene, the assays revealed a dose-dependent inhibition of telomere ladder formation, which started at 0.2 μM and was completed at 0.5 μM; in contrast, no inhibition was observed in the presence of P1, even at 10 μM (Figure 5). In addition, the other helicenes described in Figure 2 did not inhibit telomerase activity (Supporting Information Figure S3). These results indicate clearly that M1 enantioselectively bound to single-stranded telomeric DNA and stabilized the G-quadruplex structure, which resulted in telomerase inhibition.

The preference of M1 for the G-quadruplex structure arose from the orientation of the left-handed helicene and shape complementarity with the dimer G-quadruplexes. To investigate the mechanism underlying the preferential binding of M1 to G-quadruplexes, a molecular model of the M1–DNA complex was estimated using energy minimization (Figure 6). We noted that a pocket was generated by the TTA linker, the two terminal G-tetrads of the dimer G-quadruplex,[43] and the TTA loops (Figure 6a). This suggests that M1 (with a shorter linker) was readily accommodated in the pocket, without any steric hindrance, whereas the helicenes M2, M3, P2, and P3, which

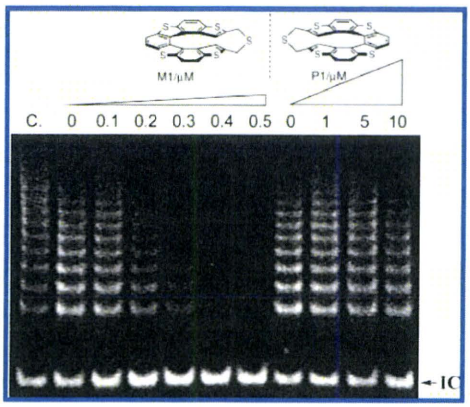

Figure 5. Inhibition of telomerase activity by M1 and P1 in vitro. Increasing concentrations of M1 (0–0.5 μM) or P1 (0–10 μM) solutions were added to the telomerase extract. The elongated products were amplified using PCR, which was followed by polyacrylamide gel electrophoresis. Lane C is a positive control, in which the buffer did not contain dimethyl formamide (DMF). The position of the internal standard is indicated as IC.

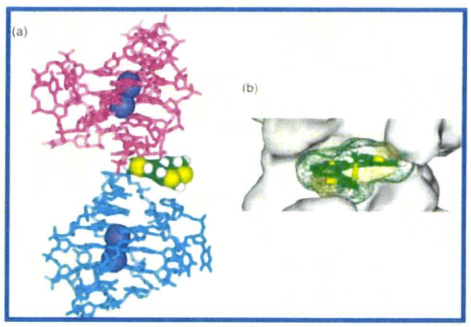

Figure 6. (a) Overall view of the energy-minimized structure of the complex formed by the G-quadruplex dimer[43] and M1. The dimer G-quadruplex structure is shown as a stick model (magenta and cyan), with M1 colored according to atom type. The K atoms in the central channel of the G-quartet are shown in blue. (b) Surface representation shows M1 (in stick representation) positioned in the cleft pocket.

contained longer linkers, introduced such steric clashes. Furthermore, the pocket itself had a special entrance, which suggests that the enantioselective binding of M1 may result from a preference by the cyclic helicene for snuggle binding to the cleft pocket, more so than P1 (Figure 6b). M1, which had a left-handed conformation, would be wedged tightly into this pocket (cleft), whereas P1, which had a right-handed conformation, would produce steric clashes that would prevent its burying deep within the pocket. The destruction of the pocket structure by the introduction of a longer linker (ODN 2) suggests that the cleft pocket played a role in the interaction of the helicene molecule with the G-quadruplex dimer.

Typically, the ligands of G-quadruplexes, such as telomestatin and TMPyP4, have flat structures. Our findings suggest that the dihedral angle of the helical frameworks should be considered as an important factor for the molecular design of G-quadruplex ligands in the future. The fact that M2 and M3 did not show any association to G-quadruplex DNA suggests that the dihedral angles of the cyclic molecules should be <50°. Although it remains unclear whether an angle of 22° is the most efficient, the critical angle should be close to this value. Thus, we

(53) Tatematsu, K.; Nakayama, J.; Danbara, M.; Shionoya, S.; Sato, H.; Omine, M.; Ishikawa, F. *Oncogene* **1996**, *13*, 2265–2274.
(54) Krupp, G.; Kuhne, K.; Tamm, S.; Klapper, W.; Heidorn, K.; Rott, A.; Parwaresch, R. *Nucleic Acids Res.* **1997**, *25*, 919–921.
(55) Gomez, D.; Mergny, J. L.; Riou, J. F. *Cancer Res.* **2002**, *62*, 3365–3368.

proposed a new ligand model for G-quadruplex-binding compounds based on insights collected from a chiral wedge molecule.

Conclusions

We found that a cyclic helicene with a short linker exhibited enantioselective binding to telomere repeats and enantioselective inhibition of telomerase. To the best of our knowledge, this is the first report demonstrating that a cyclic helicene has the properties of an enantioselective ligand that is capable of binding to telomeric G-quadruplexes. These results provide a proof-of-concept for small-molecule inhibitors of telomerase. The rational structure-based design of telomerase inhibitors necessitates a molecular understanding of the range of G-quadruplex topologies of serial G-quadruplex structures. Although we did not identify the actual models of binding of M1 to G-quadruplexes, our findings imply that the characteristics of ligands that stabilize G-quadruplexes can now be rationalized further.

Materials and Methods

Compounds and Oligonucleotides. Biotinylated DNA was purchased from Japan Bio Service Co. Ltd. The other unmodified DNA was purchased from Sigma Aldrich Japan. Those oligonucleotides were used without further purification. The synthesis of the helicene molecules was described previously.[52]

CD Measurements. CD spectra were measured using an AVIV Model 62 DS/202 CD spectrophotometer. CD spectra were recorded using a 1 cm path-length cell. Solutions for CD spectra were prepared as 0.4 mL samples of 3 μM of M and P helicenes, in the presence or absence of ODN 1 (1.5 mM strand concentration) in 2 mM K-cacodylate buffer (pH 7.0), in the presence of 150 mM KCl.

Fluorescence Measurements. Fluorescence spectra were measured using a JASCO FP-6300 spectrofluorometer. The samples were excited at 330 nm, and the fluorescence emission spectra were collected in the wavelength range of 350−550 nm. Solutions for fluorescence spectra were prepared as 0.1 mL samples at 1.0 μM of M1 and P1 in 2 mM K-cacodylate buffer (pH 7.0), in the presence or absence of ODN 1 and ODN 2 in 100 mM KCl.

SPR Assay. SPR experiments were performed using a BIACORE X instrument. The biotinylated ODN 1 (5′-biotin-TTTTTAGGG(TTAGGG)$_3$TTAGGG(GGGTTA)$_3$-3′), ODN 2 (5′-biotin-TTTTTAGGG(TTAGGG)$_4$(TTA)$_4$GGG(TTAGGG)$_3$-3′), and ODN 3 (5′-biotin-TTTTTAGGG(TTAGGG)$_4$-3′) oligos were immobilized on a streptavidin-coated sensor chip SA at a flow rate of 5 μL/min to obtain the desired immobilization levels. Experiments were performed using HBS-EP (10 mM HEPES, 150 mM NaCl, 3 mM EDTA, and 0.005% surfactant P20) buffer with 200 mM KCl and 0.1% DMF at 25 °C (pH 7.4). Sample solutions at various concentrations (0.25, 0.5, 1, 2, and 4 μM and 1 mM) were prepared in HBS-EP buffer with 200 mM KCl and 1% DMF and were injected at a flow rate of 5 μL/min. Data processing was performed by global fitting of the sensorgrams obtained experimentally to a model of 1:1 Langmuir binding using the BIAevaluation 4.1 software.

Molecular Modeling Studies. Minimizations were performed using the Discover software (MSI, San Diego, CA) with CFF force-field parameters. The starting structure was built on the basis of the recent molecular dynamics simulation.[43] K cations were placed at the bifurcating position of the O−P−O angle, at a distance of 2.51 Å from the phosphorus atom. The resulting complex was soaked in a 10 Å layer of water. The whole system was minimized without any constraint to a stage where the rms was below 0.001 kcal/mol Å.

Cell Culture. Jurkat cells, which are human T-cell leukemia lymphoblast cells, were grown in RPMI1640 (Nacalai Tasque) supplemented with 10% fetal bovine serum (JRH Biosciences), 100 U/mL penicillin, and 100 μg/mL streptomycin at 37 °C in a 5% CO_2 atmosphere.

Telomerase Activity Assay—Stretch PCR. Telomerase activity in the presence of each helicene was evaluated using the stretch PCR[53] method on a TeloChaser system (Toyobo), according to the manufacturer's instructions, with minor modifications. Briefly, Jurkat cells were collected by centrifugation at 1000g for 5 min at 4 °C and washed twice with phosphate buffered saline (PBS: 140 mM NaCl, 2.7 mM KCl, 10 mM Na_2HPO_4, 1.8 mM KH_2PO_4, pH 7.3). To extract telomerase, cells were then treated with lysis solution at a concentration of 2.5×10^4 cells/μL. Forty microliters of the reaction mixtures, including 1.0 μL of the cell extract and 1.0 μL of helicene/*N,N*-DMF solution, was incubated at 37 °C for 45 min. Thirty cycles of PCR consisting of denaturing at 95 °C for 30 s, annealing at 68 °C for 30 s, and extension at 72 °C for 45 s were performed after the purification steps. The PCR products were electrophoresed in a 10% nondenaturing polyacrylamide gel in 0.5× buffer (45 mM Tris-HCl, 45 mM boric acid, 1 mM EDTA), followed by visualization by ethidium bromide staining.

Acknowledgment. This study was supported by a Grant-in-Aid for Priority Research from the Ministry of Education, Science, Sports, SORST, and CREST of the Japan Science and Technology (JST). The authors acknowledge the support by the Global COE Program "Integrated Materials Science". We also thank Dr. John O. Trent and Dr. Jonathan B. Chaires for coordinates of the Hybrid-12 model.

Supporting Information Available: Fluorescence spectra of (M)-A and (P), and SPR sensorgram of the interaction of (a) M1 and (b) P1 with ODN 3, and telomerase activities in the presence of the helicenes. This material is available free of charge via the Internet at http://pubs.acs.org.

JA9088971

Cancer Science
The official journal of the Japanese Cancer Association

Establishment of functional telomerase immortalized human hepatocytes and a hepatic stellate cell line for telomere-targeting anticancer drug development

Koji Waki,[1] Kumiko Anno,[2] Taeko Ono,[2] Toshinori Ide,[2] Kazuaki Chayama[1] and Hidetoshi Tahara[2,3]

[1]Division of Frontier Medical Science Programs for Biomedical Research, Department of Medicine and Molecular Science and [2]Department of Cellular and Molecular Biology, Graduate School of Biomedical Sciences, Hiroshima University, Hiroshima, Japan

(Received November 23, 2009/Revised March 13, 2010/Accepted March 16, 2010/Accepted manuscript online March 23, 2010/Article first published online April 27, 2010)

We previously reported that the telomere-targeting drug telomestatin induces apoptosis accompanied by G-tail reduction and dissociation of binding protein TRF2 from telomeres in cancer cell lines but not normal or human telomerase reverse transcriptase (hTERT)-immortalized cells. Because telomere-targeting drugs induce growth arrest in normal cells at higher doses, their development is dependent on the ability to predict toxicity before *in vivo* use, but no models for this are available. Here, we established two new cell lines, telomerase immortalized human fetal hepatocytes, Hc3716-hTERT, and telomerase immortalized hepatic stellate cells, NPC-hTERT. Examinations showed that Hc3716-hTERT maintained normal mammalian cell morphology, cell growth, albumin expression, and wild-type p53 responsiveness, whereas NPC-hTERT maintained hepatic stellate-like morphology, expression of hepatic stellate markers, α-smooth muscle actin, and secretion of type I collagen, an extracellular matrix protein. Given our finding that telomere G-tail length in Hc3716 cells was decreased in senescence and increased by hTERT infection, we next examined the effect of high-dose telomestatin-induced telomere dysfunction and G-tail shortening on cellular functions in Hc3716-hTERT cells. Interestingly, telomestatin decreased expression of cytochrome P450 (CYP) family members CYP3A3/4, CYP3A5, and CYP3A7, mRNA and induced albumin expression at both mRNA and protein levels. These gene expression responses to telomestatin were similar to those of the normal parental cell Hc3716. These established cell lines thus represent the first model for predicting the side-effects of telomere-targeting drugs in normal cells, and should be powerful tools in the development of these drugs. (*Cancer Sci* 2010; 101: 1678–1685)

Telomeres are special structures at the end of eukaryotic chromosomes that play a role in chromosome end protection.[1,2] The first G-rich telomere repeat sequences, 5′-(TTGGGG)n-3′, were discovered in Tetrahymena by Blackburn.[3] Telomeric DNA in humans consists of 5′-(TTAGGG)n-3′ repeats, followed by a G-rich single-stranded 3′-overhang, the so-called telomere G-tail.[4] The telomere is gradually shortened with cell division due to problems with end-replication. Telomere repeat sequences are synthesized by telomerase, a cellular ribonucleoprotein reverse transcriptase.[5] Expression of the human telomerase catalytic subunit gene, *hTERT*, correlates with the presence of telomerase activity in human cells,[6,7] and introduction of the *hTERT* gene alone into normal cells is sufficient to induce telomerase activity, followed by telomere elongation and cell immortalization, without damage to the genome.[8,9] The status of changes in the G-tail has been controversial, with one study reporting shortening at replicative senescence,[10] and another reporting the maintenance of length in human fibroblasts at senescence.[11] Our method to determine G-tail length using the G-tail telomere hybridization protection assay (HPA)[12] showed that G-tail length in normal fibroblasts and HUVEC cells gradually shortens with cell division, but that introduction of the *hTERT* gene induces G-tail length elongation in these hTERT-infected cells.[13] However, little is known about G-tail length alterations in human hepatocytes during replicative senescence or after hTERT infection.

G-quadruplex structures are special secondary structures consisting of guanine-rich DNA sequences such as telomeres and other important regulatory regions. Telomere G-tails can adopt a G-quadruplex conformation both *in vitro* and *in vivo*, and many leading compounds targeting G-quadruplex structures have been reported to have anticancer effects. Telomestatin, originally isolated as a highly potent telomerase inhibitor from *Streptomyces anulatus 3533-SV4*,[14] enhances the stabilization of telomeric G-quadruplex DNA,[15] and has 70-fold higher selectivity for G-quadruplex DNA over duplex DNA. Telomestatin induces telomere dysfunction through t-loop destruction, and might therefore be useful in determining G-tail function.

We previously reported that telomestatin rapidly induces apoptosis in cancer cells at concentrations that do not cause normal cells to die, and that this process is accompanied by dissociation of telomere-binding protein TRF2 from telomeres in cancer cells.[16] These characteristics may suggest the potential of telomestatin as a telomere-targeting anticancer drug. Although little is known about its effects in normal cells, higher doses induce cell growth arrest. Given that the telomere capping structure, the t-loop, is essential to chromosome maintenance as well as genomic stability in both normal and cancer cells, the ongoing development of telomere-targeting anticancer drugs depends on the availability of new cellular models able to evaluate the characteristics of normal cells under the induction of telomere dysfunction using higher doses of G-quadruplex DNA stabilizers, such as telomestatin. The many types of normal cultured cells now available are not suitable for this use because of their relatively rapid mortality and accompanying loss of normal functions, and new models have thus been sought.

Cultured human hepatocytes have broad research and clinical potential. Although several published works have reported long-term culture, this is generally considered difficult in both rodent and human hepatocytes.[17,18] Several recent studies succeeded in establishing immortalized human hepatocytes by introduction of the *hTERT* gene.[19,20] However, the relation between cell proliferation and G-tail length and cellular function in hTERT-immortalized human hepatocytes is still unknown. Furthermore, little is known about the effect of telomere-targeting drugs on the cellular function of these cell lines and their usefulness for toxicity testing, which may assist the prediction of side-effects *in vivo*.

[3]To whom correspondence should be addressed.
E-mail: toshi@hiroshima-u.ac.jp

doi: 10.1111/j.1349-7006.2010.01576.x

Here, we established immortalized fetal hepatocyte and hepatic stellate cell lines using a retroviral vector expressing only hTERT. We then investigated the cellular function of these hTERT immortalized hepatocytes, as well as the effect of telomestatin as a model telomere-targeting drug on cellular function, including cell growth and hepatic functions such as expression of the cytochrome P450 (CYP) superfamily and albumin (ALB).

Materials and Methods

Cell culture and drug treatment. Human fetal hepatocytes (Hc3716) were obtained from Applied Cell Biology Research Institute (Kirkland, WA, USA) (Data S1).

***hTERT* gene transduction by retroviral method.** To produce retrovirus supernatants, pMSCV-puro-hTERT or pFB-neo-hTERT retrovirus constructs were transfected into the PT67 packaging cell line (Takara Bio USA, Madison, WI, USA) with the FuGENE6 transfection reagent (Roche Diagnostics, Mannheim, Germany). After 2 days, the supernatants were collected and passed through a 0.22 μm filter (Millipore, Billerica, MA, USA) after adding polybrene at a final concentration of 6 μg/mL. Filtered supernatants were then used to infect the target cell. Retrovirus supernatants from pMSCV-puro-hTERT were used to infect human fetal Hc3716 hepatocytes. Retrovirus supernatants from pFB-neo-hTERT were used to infect non-parenchymal cells (NPC). After 24 h of incubation with these viruses, the medium was replaced with fresh complete medium containing puromycin (0.7 μg/mL) or G-418 (600 μg/mL).

Telomerase assay. Telomerase activity was measured by modified telomere repeat amplification protocol (TRAP) as described previously Data S1.[21]

Telomere length assay by Southern blot analysis. Genomic DNA was purified from cells using phenol–chloroform extraction. Purified DNA was then digested with *Hinf* I restriction enzyme, and run on 0.9% agarose gel with 0.5 × TBE buffer. Telomere length was measured using the TeloTAGGG telomere length assay kit according to the manufacturer's instructions (Roche Diagnostics).

Quantification of telomere length and telomere G-tail length by G-tail telomere hybridization protection assay. G-tail length was measured using the G-tail telomere hybridization protection assay.[12] Quantification of total telomere length (both double-stranded and single-stranded) was carried out using telomere HPA methods as described previously.[22] For the telomere G-tail assay, 5 μg non-denatured DNA was used to measure the G-tail, and 0.5 μg denatured DNA was used to measure total telomere length. To normalize the luminescence of each sample, we took 1 μL from each sample tube and measured the DNA amount using NanoDrop (ND-1000; Thermo Fisher Scientific Inc., Waltham, MA, USA). Probes for AE-labeling of telomeres were supplied by Fujirebio (Tokyo, Japan).

RNA isolation and RT-PCR. Total RNA was extracted using TRIzol reagent (Life Technologies Co., Carlsbad, CA, USA) in accordance with the manufacturer's instructions Data S1.

Western blot analysis. Monoclonal antibodies against human proteins and their dilution were as follows: ALB (1:1000) (Sigma, Aldrich Co., St Louis, MO, USA); α-fetoprotein (AFP; 1:1000) (Sigma); cytokeratin8 (CK8; 1:1000) (Sigma); cytokeratin18 (CK18; 1:4000) (Sigma); α-smooth muscle actin (αSMA; 1:1000) (Sigma); p53 (1:400) (Upstate Biotechnology, Lake Placid, NY, USA); p21 (1:2000) (Upstate Biotechnology, Millipore, Billerica, MA, USA); and β-actin (1:10 000) (Sigma). The polyclonal antibody was cyclin dependent kinase4 (CDK4)

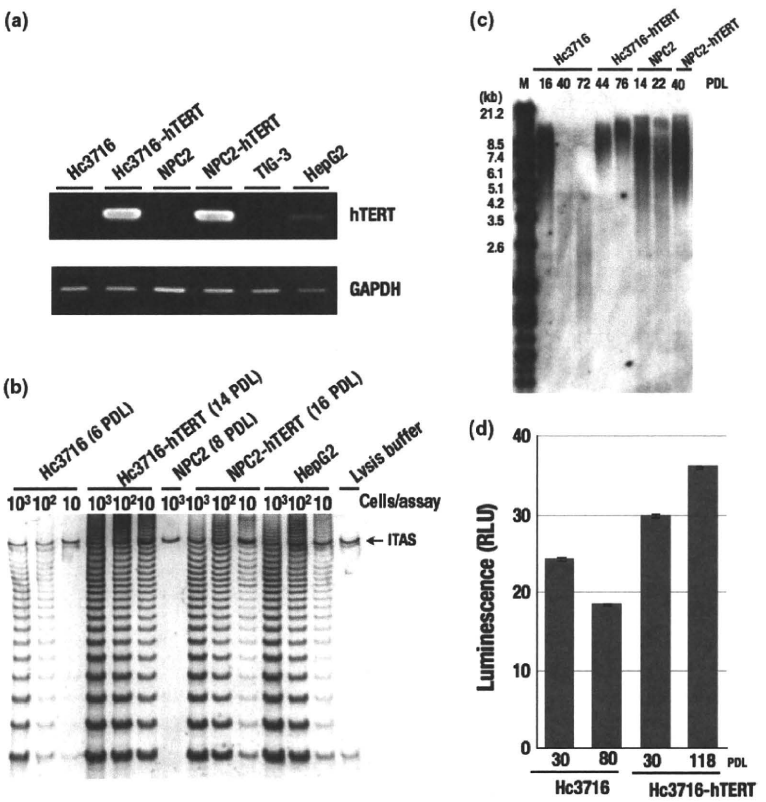

Fig. 1. Telomerase activity and human telomerase reverse transcriptase (hTERT) mRNA expression in hTERT-infected cells. (a) Expression of hTERT mRNA by RT-PCR in parental cells and hTERT-infected cells. GAPDH was used as an internal control. Hc3716, human fetal hepatocytes; HepG2, a telomerase-positive hepatoma cell line used as a control; NPC2, non-parenchymal cells; TIG-3, telomerase-negative normal human fetal fibroblasts. (b) Telomerase activity was measured by telomere repeat amplification protocol assay. ITAS, internal telomerase assay standard. (c) Telomere length analysis in hTERT-infected cells. A Southern blot analysis for terminal-restriction fragment TRF was carried out on parental and hTERT-infected cells at different population doubling levels (PDL). M, marker. (d) Telomere G-tail length in Hc3716 and Hc3716-hTERT cells. Hc3716 (30 PDL) was used for young cells, and Hc3716 (80 PDL) for senescent cells. RLU, relative light unit.

(1:500) (Santa Cruz Biotechnology, Santa Cruz, CA, USA) Data S1.

Results

Establishment of hTERT-infected human hepatocytes and NPC. To establish hTERT immortalized hepatocytes and NPC, hTERT retrovirus was infected into human Hc3716 hepatocytes at nine population doubling levels (PDL), and NPC cells at eight PDL. The resulting antibiotic-resistant cells were obtained as hTERT hepatocytes and hTERT-NPC cells. These hTERT-infected cells, Hc3716-hTERT and NPC2-hTERT, showed high levels of hTERT mRNA using RT-PCR (Fig. 1a). Evaluation of telomerase activity by a modified TRAP assay (Fig. 1b) showed that control Hc3716 (six PDL) cells had low telomerase activity, whereas hTERT-infected cells showed strong activity. Having established that hTERT infection successfully reconstituted telomerase activity in Hc3716-hTERT and NPC-hTERT cells, we assessed telomere length by Southern blot analysis (Fig. 1c). Terminal restriction fragment (TRF) length analysis indicated that telomeres were lengthened in the hTERT-infected cells compared with non-infected normal cells (Fig. 1c). Although telomere length is known to decrease with cellular senescence in human hepatocytes, technical difficulties have prevented close investigation of G-tail length, and to our knowledge no studies have been reported. We therefore measured telomere G-tail length using our novel, previously developed method, G-tail telomere HPA.[12] Results showed that telomere G-tail length decreased with senescence, but was elongated in hTERT-infected Hc3716 cells (Fig. 1d).

Growth characteristics and cell morphology in hTERT hepatocytes and hTERT NPC cells. We first cultured human fetal hepatocytes with a Hepatocyte Medium BulletKit (Cambrex Co., Charles City, IA, USA) containing 10% FBS but without human serum (HS). These divided for several passages only and then rapidly stopped proliferating, before finally detaching from the dish. After optimization for O_2 concentration, culture dish, feeder layer culture, and serum species, we found that human serum was the key factor for the maintenance of human hepatocytes. From these trials we formulated a culture medium that effectively supports the growth of human hepatocytes, which we termed the ''hepatocytes medium kit'' containing 5% FBS and 10% HS.

To examine the ability of Hc3716-hTERT and NPC-hTERT to bypass replicative senescence, we cultured control Hc3716, Hc3716-hTERT, control NPC, and NPC-hTERT with 5% FBS and 10% HS culture medium. After 86–90 PDL, cell proliferation virtually ceased in control Hc3716 with entry into replicative senescence (Fig. 2a). When cultured without 10% HS, the proliferation potential of Hc3716 and Hc3716-hTERT dramatically decreased, and finally the cells stopped growing (data not shown). In contrast, Hc3716-hTERT grew at a similar rate to Hc3716 and actively doubled to the last count of the study at day 800 (population doubling approximately every 2.5 days).

Hc3716 showed a typical cobblestone-like morphology when in a confluent monolayer (Fig. 2b). The cells became flattened and enlarged as the number of passages increased, particularly after 86 PDL. Hc3716-hTERT showed a similar morphology in a confluent monolayer and appeared to be in a state of contact inhibition of growth, because they did not pile up on each other.

Cell proliferation virtually ceased in control NPC after 30 PDL. In NPC-hTERT, however, proliferation continued for more than 50 PDL (approximately one population doubling every 4 days) (Fig. 2c). NPC-hTERT appeared closely similar to non-infected cells and NPC cells and NPC-hTERT showed a typical spindled morphology (Fig. 2d). Taken together, these characteristics, including cell growth, contact inhibition, and cell morphology, showed that the Hc3716-hTERT and NPC-hTERT

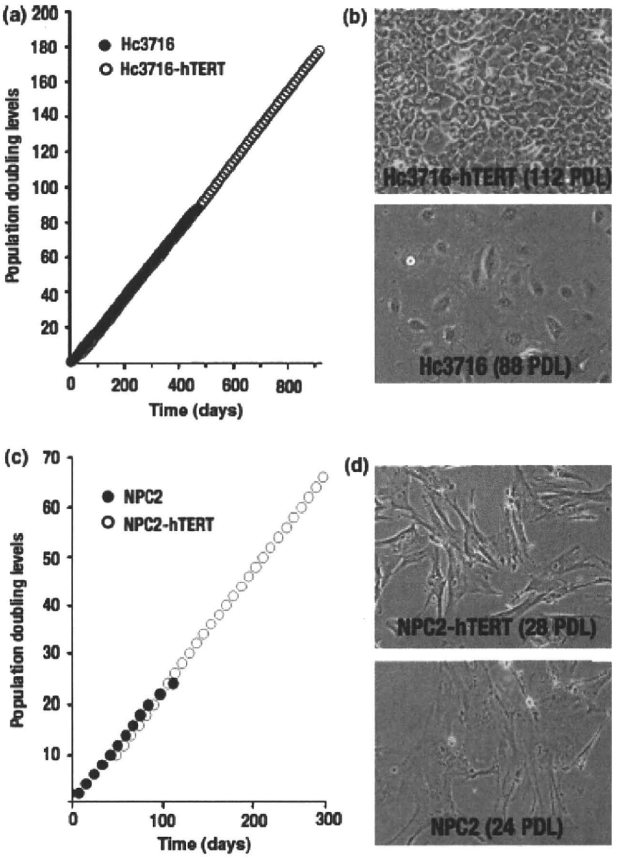

Fig. 2. Morphology and growth curve of parental cells and human telomerase reverse transcriptase (hTERT)-infected cells. (a) Cumulative growth curve in Hc3716 human fetal hepatocytes and Hc3716-hTERT. (b) Morphology of Hc3716 [88 population doubling levels (PDL); senescent state] and Hc3716-hTERT (112 PDL). (c) Cumulative growth curve in normal non-parenchymal cells (NPC2) and NPC2-hTERT. (d) Morphology of NPC2 (24 PDL; senescent state) and NPC2-hTERT (28 PDL).

lines were normal hepatocytes and NPC-like cells, respectively, with normal cell-like characteristics.

Hc3716-hTERT expressed ALB but not AFP. To determine whether Hc3716-hTERT had the functional properties of hepatocytes, we examined the expression of several hepatic marker proteins, ALB, AFP, CK8, and CK18 by Western blot analysis. AFP and ALB are the first secreted proteins produced by the embryonic liver, whereas CK8 and CK18 are expressed in adult hepatocytes. To examine ALB expression, cells were washed with PBS three times to remove human ALB derived from HS, cultured in media without HS for 3 days, and detected by Western blot analysis. Hc3716-hTERT (40 PDL) expressed much more ALB than control Hc3716 (40 PDL) (Fig. 3a). AFP expression was not detected in either Hc3716-hTERT or Hc3716, whereas the hepatic cancer cell line HepG2 expressed AFP at high levels (Fig. 3b). Hc3716-hTERT (40 PDL) as well as control Hc3716 also expressed either CK8 or CK18 but not AFP, a marker of immature or tumorous hepatocytes such as HepG2. NPC-hTERT did not express CK8 or CK18 (Fig. 3c).

We also examined the expression of hepatocyte nuclear factor (HNF)4 and CYP3A7 mRNA by RT-PCR (Fig. 4a). Hepatocyte nuclear factor 4 is well known as a liver-enriched differentiation factor, whereas CYP3A7, originally isolated from fetal liver,[23]

doi: 10.1111/j.1349-7006.2010.01576.x

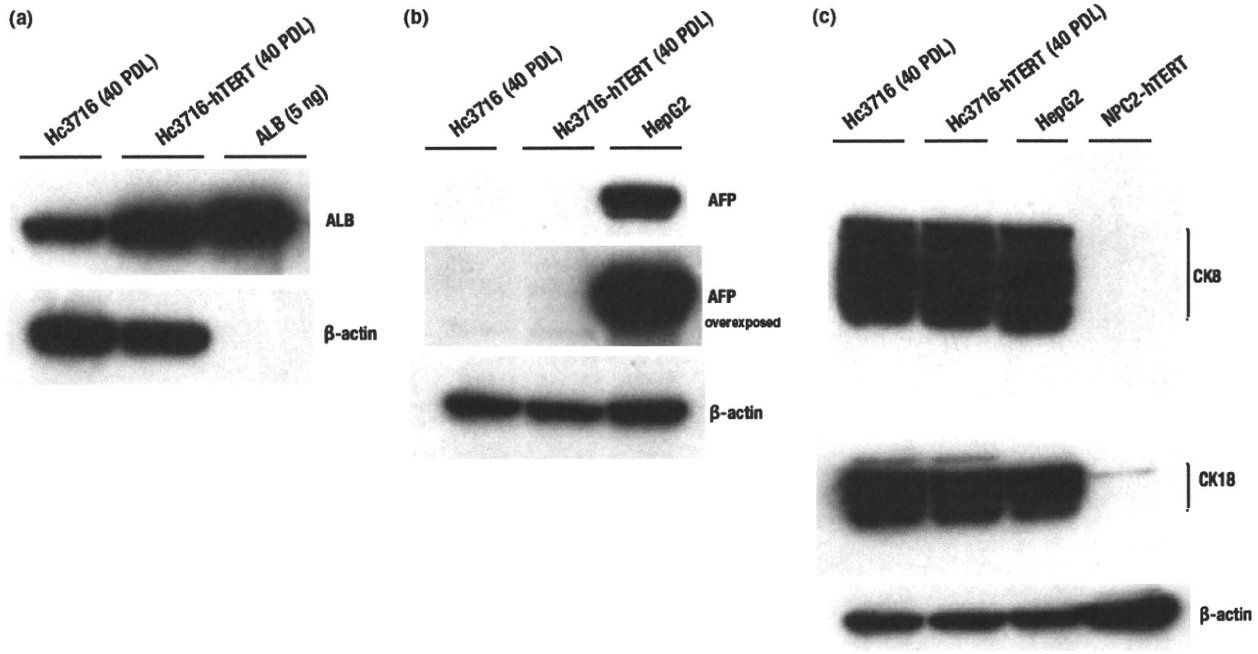

Fig. 3. Characterization of human fetal hepatocytes (Hc3716) and telomerase immortalized human fetal hepatocytes (Hc3716-hTERT). (a) Protein expression of albumin (ALB) in Hc3716 and Hc3716-hTERT were examined by Western blot analysis. Purified ALB (5 ng) was used as a positive control. (b) Protein expression of α-fetoprotein (AFP) in Hc3716 and Hc3716-hTERT was examined by Western blot analysis. HepG2, hepatoma cell line used as a positive control. (c) Protein expression of cytokeratin8 (CK8) and cytokeratin18 (CK18) in Hc3716 and Hc3716-hTERT were examined by Western blot analysis. β-actin was used as a loading control.

accounts for up to 50% of total fetal hepatic CYP content.[24] Although expression of HNF4 and CYP3A7 was not detected in proliferating states, both mRNA were induced when the cells reached confluence (Fig. 4a). Moreover, CYP3A4 and CYP3A7 are known to be induced by nifedipine and rifampicin. Induction of CYP3A4 and CYP3A7 by these compounds was partial in normal Hc3716 cells, but both CYP3A4 and CYP3A7 were up-regulated in Hc3716-hTERT (Fig. 4b), suggesting that Hc3716-hTERT maintains normal hepatocyte characteristics.

Characterization of NPC-hTERT. To determine the characteristics of NPC-hTERT, we examined the expression of αSMA, a marker for activated hepatic stellate cells (HSC) by Western blot analysis. Human HSC strain LI90, established from a mesenchymal liver tumor of a 55-year-old Japanese woman,[25] was used as the positive control in the present study. NPC-hTERT (26 PDL) as well as untransduced NPC (14 PDL) also expressed αSMA, whereas Hc3716-hTERT (40 PDL) did not (Fig. 5a).

Hepatic stellate cells constitute a major cell type responsible for liver fibrosis following their activation into fibrogenic myofibroblast-like cells.[26–29] Activated HSC are considered the major source of extracellular matrix in hepatic fibrosis.[30] Following liver injury, HSC undergo an activation process in which quiescent vitamin A storing cells transform into proliferative, smooth muscle actin-positive myofibroblast-like cells that secrete extracellular matrix proteins, especially type I collagen.[26] We examined the expression of collagen type I mRNA and HGF mRNA in NPC-hTERT (26 PDL) by RT-PCR and compared it with NPC (14 PDL) (Fig. 5b). Expression levels of collagen type I mRNA and HGF mRNA in NPC-hTERT (26 PDL) were similar to those of NPC (14 PDL), whereas Hc3716-hTERT did not express collagen type I mRNA. From these results, we identified NPC and NPC-hTERT as HSC.

HC3716-hTERT cells maintain p53-dependent DNA damage signals, similar to normal Hc3716 hepatocytes. To study the molecular basis of DNA damage response to topoisomerase poison, normal and hTERT-infected cells were treated with the indicated concentrations of adriamycin for 24 h. p53 proteins were accumulated in response to adriamycin (a topoisomerase II inhibitor) in a dose-dependent manner in both normal and hTERT-infected cells, including Hc3716-hTERT and NPC-hTERT (Fig. 6). As expected, the p53 target, cyclin-dependent kinase inhibitor p21waf1/cip1/sdi1, was also induced by adriamycin in hTERT-infected cells (Fig. 6). We found that Hc3716-hTERT and NPC-hTERT maintained wild-type p53.

Telomestatin inhibits cell growth in Hc3716-hTERT cells. Telomestatin is known to induce telomere dysfunction by destruction of the telomere t-loop structure through binding to the G-quadruplex structure of the G-tail. We reported that cancer cell lines were sensitive to apoptosis by telomestatin treatment.[16] Although the mechanism of this difference in sensitivity between normal cells and a cancer cell line is still unclear, higher doses of telomestatin treatment might induce telomere dysfunction, accompanied by G-tail reduction. To examine the effect of telomere dysfunction on cellular functions of Hc3716-hTERT, we used telomestatin as an inducer of telomere dysfunction through G-tail reduction. To determine the effects of telomestatin on cell growth, Hc3716-hTERT cells were cultured in the presence of telomestatin at concentrations of 0, 5, and 25 μM for 5 days. When Hc3716-hTERT cells were treated with telomestatin at 25 μM, the cells ceased growing and cell death was induced. G-tail lengths were examined by G-tail telomere HPA (Fig. 7a). Total telomere length was also examined using HPA assay with the denaturation of genomic DNA before assay (Fig. 7b). When Hc3716-hTERT cells were treated with telomestatin at 25 μM for 5 days, a remarkable reduction in G-tails was observed (Fig. 7a). We also measured total telomere length using the telomere HPA. Results showed no significant difference in total telomere length after treatment with telomest-

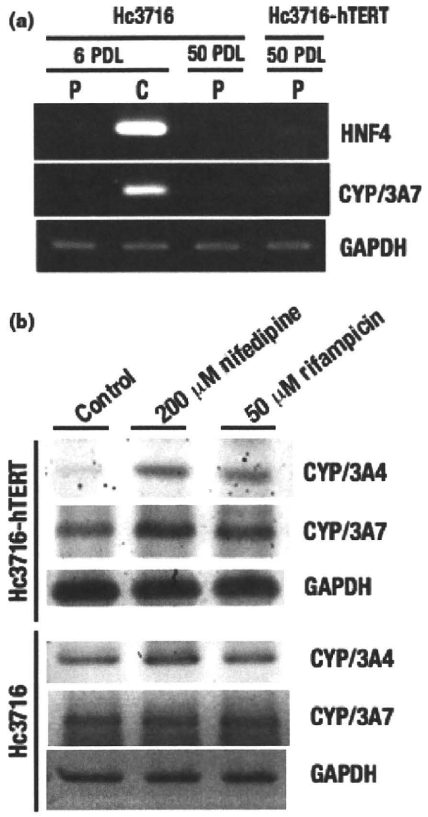

Fig. 4. (a) mRNA expression of hepatocyte nuclear factor 4 (HNF4) and cytochrome P450 (CYP)/3A7 in normal human fetal hepatocytes (Hc3716) and those infected with human telomerase reverse transcriptase (Hc3716-hTERT) were examined by RT-PCR. C, confluent monolayers; P, proliferative phase. (b) Induction of CYP/3A4 and CYP/3A7 after treatment with nifedipine and rifampicin in Hc3716 and Hc3716-hTERT was examined by RT-PCR. GAPDH was used as an internal control. Control, no treatment.

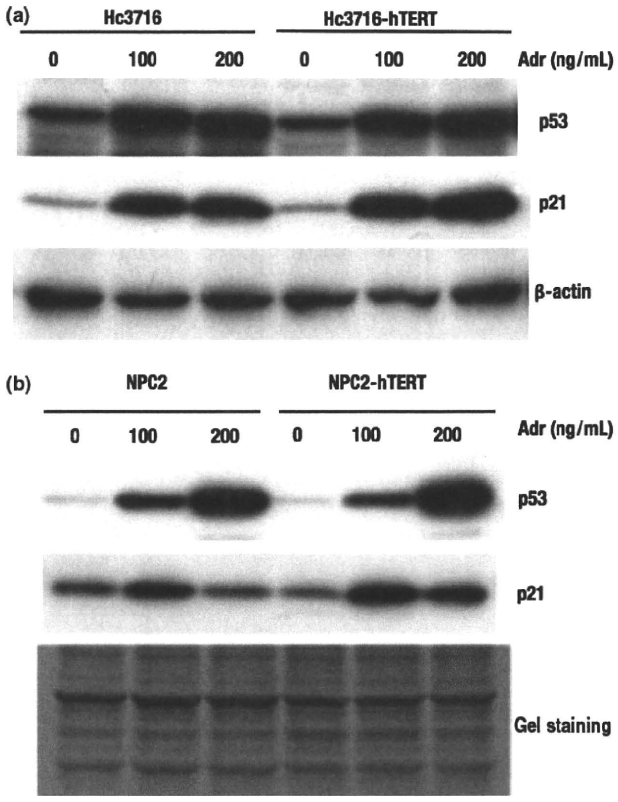

Fig. 6. DNA damage response to topoisomerase poison in human telomerase reverse transcriptase (hTERT)-infected cells. (a) Accumulation of p53 and induction of p21 in normal (Hc3716) and infected (Hc3716-hTERT) human fetal hepatocytes were examined by Western blot analysis. Adr, adriamycin. (b) Accumulation of p53 and induction of p21 in normal (NPC2) and infected (NPC2-hTERT) non-parenchymal cells were examined by Western blot analysis. Gel staining, loading control.

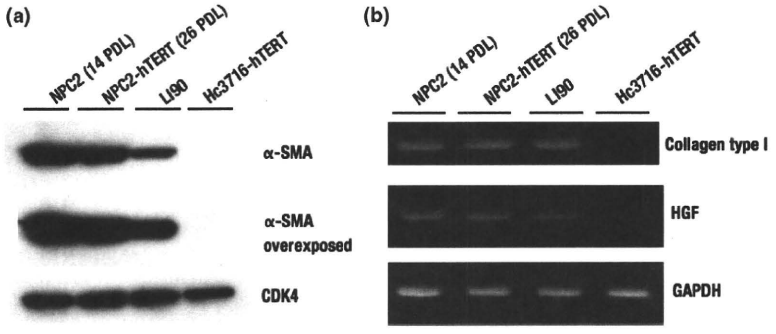

Fig. 5. (a) Characterization of normal non-parenchymal cells (NPC2) and those infected with human telomerase reverse transcriptase (NPC2-hTERT). Protein expression of α-smooth muscle actin (α-SMA) in NPC2 and NPC2-hTERT were examined by Western blot analysis. Cyclin dependent kinase 4 (CDK4) was used as an internal control. LI90, hepatic stellate cell line derived from mesenchymal liver tumor. (b) mRNA expression of collagen type I and hepatocyte growth factor (HGF) in NPC2 and NPC2-hTERT was examined by RT-PCR. GAPDH was used as an internal control.

atin for 5 days (Fig. 7b), which is similar to the findings with cancer cells. Telomestatin did not affect total telomere length, but G-tail lengths were decreased by treatment with telomestatin at 25 μM in Hc3716-hTERT cells, suggesting that high doses of telomestatin can induce telomere dysfunction through G-tail reduction in Hc3716-hTERT.

Hc3716-hTERT cells showed similar characteristics of CYP expression in response to telomestatin. To determine whether G-tail length affects the function of Hc3716-hTERT cells, expression of ALB and the CYP family was examined by RT-PCR and Western blot analysis after treatment with telomestatin at 0, 5, and 25 μM. Unexpectedly, the ALB expression level increased with increasing telomestatin concentration at both the mRNA and protein levels (Fig. 8a). This ALB induction was also observed in parental Hc3716 cells at the mRNA level, suggesting that ALB induction by telomestatin is not due to introduction of the *hTERT* gene or elongation of telomere length. We examined CYP family expression after treatment with telomestatin in Hc3716 and Hc3716-hTERT cells, including CYP1A2, CYP2B6, CYP2C, CYP2D6, CYP2E1, CYP3A3/4,

doi: 10.1111/j.1349-7006.2010.01576.x

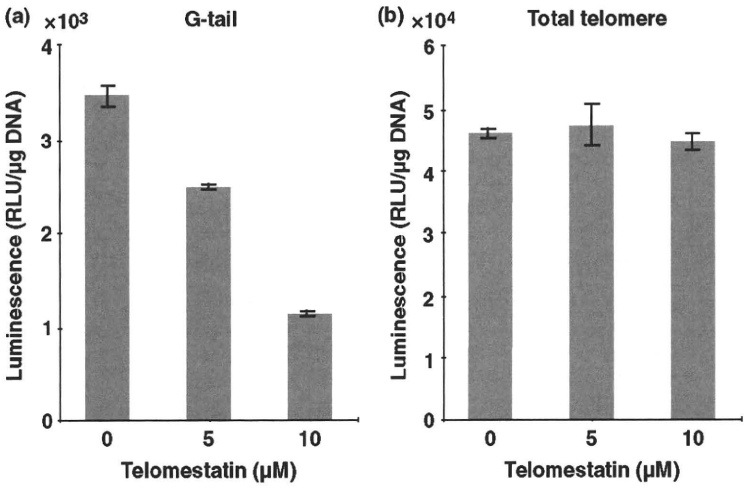

Fig. 7. Telomere G-tail length and total telomere length after treatment with telomestatin in telomerase immortalized human fetal hepatocytes (Hc3716-hTERT). (a) Telomere G-tail length in Hc3716-hTERT cells were examined by G-tail telomere hybridization protection assay. Each chemiluminescent value was calibrated with DNA content used in the assay. RLU, relative light unit. (b) Total telomere length in Hc3716-hTERT cells was examined using the telomere hybridization protection assay method. Denatured DNA (0.5 μg) was used in each assay.

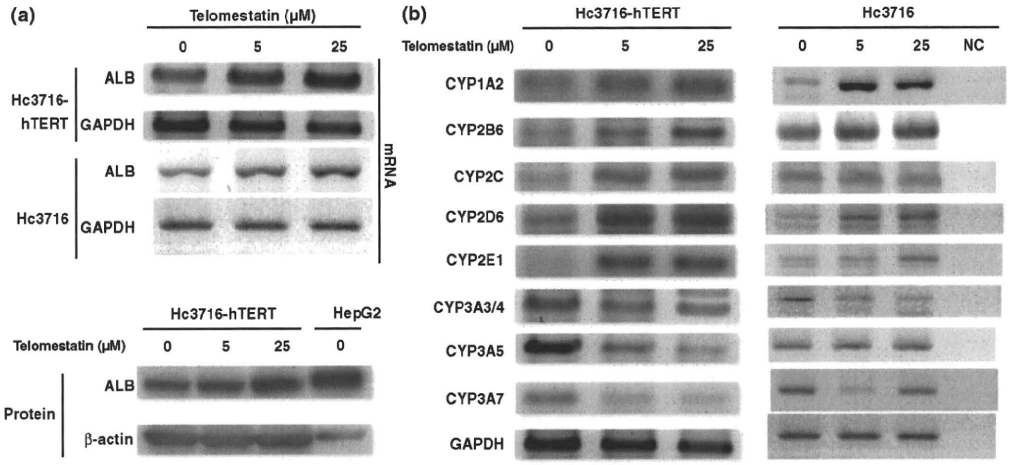

Fig. 8. (a) Expression of albumin (ALB) after treatment with telomestatin in normal (Hc3716) and telomerase immortalized (Hc3716-hTERT) human fetal hepatocytes examined by RT-PCR. Albumin protein levels in Hc3716-hTERT were examined by Western blot analysis. HepG2, hepatoma cell line used as a positive control. (b) Cytochrome P450 (CYP) induction after treatment with telomestatin in Hc3716-hTERT and HC3716 cells was examined by RT-PCR. GAPDH was used as an internal control. NC, no RNA sample as negative control.

CYP3A5, and CYP3A7. Interestingly, mRNA of CYP1A2, CYP2B6, CYP2C, CYP2D6, and CYP2E1 was strongly induced in telomestatin-treated Hc3716-hTERT cells (Fig. 8b, left). In contrast, expression of CYP3A3/4, CYP3A5, and CYP3A7 was decreased in these cells (Fig. 8b, left), which is opposite to the effects of treatment with nifedipine or rifampicin (Fig. 4b). This CYP family response to telomestatin is similar to that in telomestatin-treated Hc3716 parental cells (Fig. 8b, right). Further examination of the molecular mechanism of these responses of the CYP family is required. CYP expression was clearly altered by telomestatin treatment, and CYP responses to telomestatin were similar to those of parental Hc3716 cells. Although concerns have been expressed that hTERT expression might affect the metabolism of compounds, no other immortalized cell line bearing characteristics of normal mammalian cells are available for use in the prediction of drug cytotoxicity. Taken together, these results suggest that our established cell line, Hc-3716-hTERT, represents a suitable tool for the prediction of drug cytotoxicity in the development of telomere-targeting anticancer drugs.

Discussion

In this study, we established human hepatocyte immortalized cells, HC3716-hTERT, and human hepatic satellite cells, NPC-hTERT, which bear characteristics of normal cells. In HC3716-hTERT, the telomere-targeting anticancer drug telomestatin decreased CYP3A3/4, CYP3A5, and CYP3A7 expression and induced ALB expression at both mRNA and protein levels, similar to the responses seen in the normal parental cell Hc3716. These findings suggest that the combination of telomestatin and Hc3716-hTERT might represent a useful new cellular model to evaluate the characteristics of normal cells, and to predict the toxicity of drugs under induction of telomere dysfunction.

Given that inappropriate culture induces senescence programming in human cells, we first optimized the culture medium for the growth and maintenance of human fetal hepatocytes by varying the concentration of FBS. The resulting culture medium contained 5% FBS and 10% HS, and effectively supported the growth of human fetal hepatocytes. Results clearly showed that normal fresh HS promoted the growth of human fetal hepato-

cytes and extended their lifespan to over 80 PDLs, compared to 10 PDLs with normal culture conditions (FBS alone). Hepatocytes finally reached senescence at 80 PDLs, at which time analysis of TRF and G-tail HPA length showed shortening of both. The average TRF in senescent Hc3716 cells with optimal culture medium was approximately 2.5 kb, which appears to be the minimum length required for proper chromosome maintenance.

We combined the use of these optimal culture conditions with forced expression of hTERT and subsequent telomerase activity to establish and immortalize the Hc3716- and NPC-based cell lines Hc3716-hTERT and NPC-hTERT. After several population doublings, TRF length and HPA analysis showed that the telomeres and G-tails in these hTERT-transduced cells were lengthened (Fig. 1c). This finding indicated that these cells were suitable for the evaluation of telomere-targeting drugs.

Although these hTERT-infected cells have an immortal phenotype, several important phenotypic characteristics of the parental cell were retained. For example, expression of CK8, CK18, CYP family, and ALB were seen in both Hc3716 and Hc3716-hTERT cells, but not in NPC-hTERT. The hTERT-infected cells did not show typical oncogenic phenotype traits such as anchorage-independent growth, contact inhibition, pile-up, or expression of mutant p53 protein. Cellular functions examined through the gene expression of hepatic markers such as CYP, CK, and ALB were more strongly maintained in the Hc3716-hTERT cells than in the parental cells, which was expected given that hepatic differential function generally decreases with proliferative aging in normal hetatocytes. Hc3716-hTERT maintained the cellular functioning of young normal hepatocytes regarding CYP, CK, and ALB expression.

NPC-hTERT showed the differential functions of HSC, including expression of collagen type I and HGF mRNA (Fig. 5b). Co-culture of Hc3716-hTERT with NPC-hTERT will help to maintain the differentiated phenotype of hepatocytes *in vitro*, for example, with regard to ALB and CYP.[31] NPC-hTERT cells can therefore be used for basic research into hepatic fibrosis.

The clinical use of telomere-targeting drugs in cancer therapy requires an understanding of their effects in normal cells, but to our knowledge, no such study or model has been reported. In this paper, we examined cell growth and hepatic function, including ALB and CYP expression, with or without telomestatin treatment, in Hc3716-hTERT cells. At higher concentrations of telomestatin, Hc3716-hTERT cells ceased proliferation, accompanied by G-tail reduction. Interestingly, total telomere length was not affected by treatment with telomestatin, suggesting that its antiproliferative effect in normal hepatocytes was induced by telomere t-loop destruction accompanied by G-tail reduction. Although we expected that ALB expression, a hallmark of hepatocytes, would be decreased by the telomere dysfunction induced by higher doses of telomestatin, we unexpectedly found that expression was increased with higher doses in hTERT hepatocytes. Although we did not undertake an *in vivo* study, we speculate that if telomestatin and other telomere-targeting drugs induce ALB expression in normal hepatocytes and secretion into blood, then the ALB level might be a candidate marker of telomere dysfunction of normal heptocytes.

The CYP family of proteins is large and ubiquitous. The proteins catalyze a multitude of reactions, including oxidation, hydroxylation, and conjugation. Depending on the specific CYP and compound, these CYP-dependent reactions may convert active compounds to the inactive state, or *vice versa*; for example, a pro-carcinogen to an active carcinogen, or a pro-drug to an active drug. Therefore, even though anticancer drugs significantly inhibit the growth of cancer, CYP-induced changes should be examined before *in vivo* application. The two models developed here might be helpful for this purpose. For example, more than 30 known pharmaceutical drugs are known to be metabolized by CYP2D6; if telomestatin is metabolized by CYP2D6, and thereby loses its antitumor activity, telomestatin might not suitable for *in vivo* application, owing to the CYP2D6 expression it induces (Fig. 8b).

Several limitations of this study warrant mention. First, CYP expression varies with race and sex, but we did not investigate these variables in the development of these models. Second, the effects of hTERT infection are not completely predictable. This unpredictability might hamper efforts to replicate our present results. Finally, the response of genes in these *in vitro* cultured cells are different from *in vivo* responses. Thus, further investigation is required to establish conclusively the usefulness of these cell lines in evaluating the toxicity of telomere-targeting drugs.

In conclusion, these new predictive models of toxicity are promising tools in the development of new telomere-targeting anticancer drugs before application to *in vivo* studies.

Acknowledgments

This work was partially supported by the Ministry of Education, Culture, Sports, Science and Technology, Japan, with a Grant-in-Aid for Scientific Research on Priority Areas (Grant No. 20014015), and the Takeda Science Foundation.

References

1 de Lange T. T-loops and the origin of telomeres. *Nat Rev Mol Cell Biol* 2004; **5**: 323–9.
2 de Lange T. Protection of mammalian telomeres. *Oncogene* 2002; **21**: 532–40.
3 Szostak JW, Blackburn EH. Cloning yeast telomeres on linear plasmid vectors. *Cell* 1982; **29**: 245–55.
4 Makarov VL, Hirose Y, Langmore JP. Long G tails at both ends of human chromosomes suggest a C strand degradation mechanism for telomere shortening. *Cell* 1997; **88**: 657–66.
5 Greider CW. Telomere length regulation. *Annu Rev Biochem* 1996; **65**: 337–65.
6 Nakamura TM, Morin GB, Chapman KB *et al.* Telomerase catalytic subunit homologs from fission yeast and human. *Science* 1997; **277**: 955–9.
7 Nakayama J, Tahara H, Tahara E *et al.* Telomerase activation by hTRT in human normal fibroblasts and hepatocellular carcinomas. *Nat Genet* 1998; **18**: 65–8.
8 Carney SA, Tahara H, Swartz CD *et al.* Immortalization of human uterine leiomyoma and myometrial cell lines after induction of telomerase activity: molecular and phenotypic characteristics. *Lab Invest* 2002; **82**: 719–28.
9 Bodnar AG, Ouellette M, Frolkis M *et al.* Extension of life-span by introduction of telomerase into normal human cells. *Science* 1998; **279**: 349–52.
10 Stewart SA, Ben-Porath I, Carey VJ, O'Connor BF, Hahn WC, Weinberg RA. Erosion of the telomeric single-strand overhang at replicative senescence. *Nat Genet* 2003; **33**: 492–6.
11 Chai W, Shay JW, Wright WE. Human telomeres maintain their overhang length at senescence. *Mol Cell Biol* 2005; **25**: 2158–68.
12 Tahara H, Kusunoki M, Yamanaka Y, Matsumura S, Ide T. G-tail telomere HPA: simple measurement of human single-stranded telomeric overhangs. *Nat Methods* 2005; **2**: 829–31.
13 Anno K, Hayashi A, Takahashi T, Mitsui Y, Ide T, Tahara H. Telomerase activation induces elongation of the telomeric single-stranded overhang, but does not prevent chromosome aberrations in human vascular endothelial cells. *Biochem Biophys Res Commun* 2007; **353**: 926–32.
14 Shin-ya K, Wierzba K, Matsuo K *et al.* Telomestatin, a novel telomerase inhibitor from Streptomyces anulatus. *J Am Chem Soc* 2001; **123**: 1262–3.
15 Tauchi T, Shin-Ya K, Sashida G *et al.* Activity of a novel G-quadruplex-interactive telomerase inhibitor, telomestatin (SOT-095), against human leukemia cells: involvement of ATM-dependent DNA damage response pathways. *Oncogene* 2003; **22**: 5338–47.
16 Tahara H, Shin-Ya K, Seimiya H, Yamada H, Tsuruo T, Ide T. G-Quadruplex stabilization by telomestatin induces TRF2 protein dissociation from telomeres and anaphase bridge formation accompanied by loss of the 3′ telomeric overhang in cancer cells. *Oncogene* 2006; **25**: 1955–66.

doi: 10.1111/j.1349-7006.2010.01576.x

17 Lazaro CA, Croager EJ, Mitchell C *et al.* Establishment, characterization, and long-term maintenance of cultures of human fetal hepatocytes. *Hepatology* 2003; **38**: 1095–106.
18 Hino H, Tateno C, Sato H *et al.* A long-term culture of human hepatocytes which show a high growth potential and express their differentiated phenotypes. *Biochem Biophys Res Commun* 1999; **256**: 184–91.
19 Wege H, Le HT, Chui MS *et al.* Telomerase reconstitution immortalizes human fetal hepatocytes without disrupting their differentiation potential. *Gastroenterology* 2003; **124**: 432–44.
20 Tsuruga Y, Kiyono T, Matsushita M *et al.* Establishment of immortalized human hepatocytes by introduction of HPV16 E6/E7 and hTERT as cell sources for liver cell-based therapy. *Cell Transplant* 2008; **17**: 1083–94.
21 Tahara H, Nakanishi T, Kitamoto M *et al.* Telomerase activity in human liver tissues: comparison between chronic liver disease and hepatocellular carcinomas. *Cancer Res* 1995; **55**: 2734–6.
22 Nakamura Y, Hirose M, Matsuo H, Tsuyama N, Kamisango K, Ide T. Simple, rapid, quantitative, and sensitive detection of telomere repeats in cell lysate by a hybridization protection assay. *Clin Chem* 1999; **45**: 1718–24.
23 Kitada M, Kamataki T, Itahashi K, Rikihisa T, Kato R, Kanakubo Y. Purification and properties of cytochrome P-450 from homogenates of human fetal livers. *Arch Biochem Biophys* 1985; **241**: 275–80.
24 Wrighton SA, Vandenbranden M. Isolation and characterization of human fetal liver cytochrome P450HLp2: a third member of the P450III gene family. *Arch Biochem Biophys* 1989; **268**: 144–51.
25 Murakami K, Abe T, Miyazawa M *et al.* Establishment of a new human cell line, LI90, exhibiting characteristics of hepatic Ito (fat-storing) cells. *Lab Invest* 1995; **72**: 731–9.
26 Friedman SL. Molecular regulation of hepatic fibrosis, an integrated cellular response to tissue injury. *J Biol Chem* 2000; **275**: 2247–50.
27 Rockey DC. Hepatic blood flow regulation by stellate cells in normal and injured liver. *Semin Liver Dis* 2001; **21**: 337–49.
28 Schuppan D, Ruehl M, Somasundaram R, Hahn EG. Matrix as a modulator of hepatic fibrogenesis. *Semin Liver Dis* 2001; **21**: 351–72.
29 Xu L, Hui AY, Albanis E *et al.* Human hepatic stellate cell lines, LX-1 and LX-2: new tools for analysis of hepatic fibrosis. *Gut* 2005; **54**: 142–51.
30 Maher JJ, McGuire RF. Extracellular matrix gene expression increases preferentially in rat lipocytes and sinusoidal endothelial cells during hepatic fibrosis in vivo. *J Clin Invest* 1990; **86**: 1641–8.
31 Bhatia SN, Balis UJ, Yarmush ML, Toner M. Effect of cell-cell interactions in preservation of cellular phenotype: cocultivation of hepatocytes and nonparenchymal cells. *FASEB J* 1999; **13**: 1883–900.

Supporting Information

Additional Supporting Information may be found in the online version of this article.

Data S1. Material and methods.

Please note: Wiley-Blackwell are not responsible for the content or functionality of any supporting materials supplied by the authors. Any queries (other than missing material) should be directed to the corresponding author for the article.

Research Paper

Cooperation of DNA-PKcs and WRN helicase in the maintenance of telomeric D-loops

Rika Kusumoto-Matsuo[1,7], Patricia L. Opresko[2], Dale Ramsden[3, 4, 5], Hidetoshi Tahara[6] and Vilhelm A. Bohr[1]

[1] Laboratory of Molecular Gerontology, National Institute on Aging, National Institutes of Health, Baltimore, MD 21224, USA

[2] Department of Environmental and Occupational Health, University of Pittsburgh Graduate School of Public Health, Pittsburgh, PA 15219, USA

[3] Department of Biochemistry and Biophysics, University of North Carolina at Chapel Hill, Chapel Hill, NC 27599, USA

[4] Curriculum in Genetics and Molecular Biology, University of North Carolina at Chapel Hill, Chapel Hill, NC 27599, USA

[5] Lineberger Comprehensive Cancer Center, University of North Carolina at Chapel Hill, Chapel Hill, NC 27599, USA

[6] Department of Cellular and Molecular Biology, Division of Integrated Medical Science, Graduate School of Biomedical Sciences, Hiroshima University, Hiroshima 734-8551, Japan

[7] Present address: Pathogen Genomics Center, National Institute of Infectious Diseases, 4-7-1 Gakuen, Musashi-murayama, Tokyo 208-0011, Japan

Running title: *DNA-PKcs stimulates WRN helicase activity*
Key words: *RecQ, WRN, DNA-PKcs, telomere, aging, DNA repair*
Correspondence: *Vilhelm A. Bohr, MD/PhD, Laboratory of Molecular Gerontology, National Institute on Aging, National Institutes of Health, 251 Bayview Blvd, Baltimore, MD 21224, USA*
Received: *04/18/10; accepted: 04/28/10; published on line: 04/30/10*
E-mail: *bohrv@nih.gov*

Abstract: Werner syndrome is an inherited human progeriod syndrome caused by mutations in the gene encoding the Werner Syndrome protein, WRN. It has both 3'-5' DNA helicase and exonuclease activities, and is suggested to have roles in many aspects of DNA metabolism, including DNA repair and telomere maintenance. The DNA-PK complex also functions in both DNA double strand break repair and telomere maintenance. Interaction between WRN and the DNA-PK complex has been reported in DNA double strand break repair, but their possible cooperation at telomeres has not been reported. This study analyzes the *in vitro* and *in vivo* interaction at the telomere between WRN and DNA-PKcs, the catalytic subunit of DNA-PK. The results show that DNA-PKcs selectively stimulates WRN helicase but not WRN exonuclease *in vitro*, affecting that WRN helicase unwinds and promotes the release of the full-length invading strand of a telomere D-loop model substrate. In addition, the length of telomeric G-tails decreases in DNA-PKcs knockdown cells, and this phenotype is reversed by overexpression of WRN helicase. These results suggest that WRN and DNA-PKcs may cooperatively prevent G-tail shortening *in vivo*.

INTRODUCTION

Werner syndrome (WS) is a hereditary disorder associated with symptoms of premature aging, including early onset of cataracts, osteoporosis, atherosclerosis and cancer [1, 2]. The cellular phenotype of WS includes premature cellular senescence, telomere dysfunction and chromosome instability. WS is caused by mutations in the gene encoding the Werner syndrome protein (WRN), a multifunction protein that possesses 3'-5' DNA helicase, 3'-5' DNA exonuclease, branch migration, and strand annealing activities [3-8]. WRN helicase is active on a wide variety of DNA substrates, with preference for forked duplex molecules and structures at telomeric DNA [9].

Telomeres are nucleoprotein structures at the ends of eukaryotic chromosomes. In humans, telomeric DNA includes a duplex region containing tandem repeats of the sequence 5'-TTAGGG-3' and telomeric 3'-G-overhang, so called G-tail. The telomere DNA loops back on itself forming a lariat t-loop structure, where the G-tail invades the duplex telomeric repeats and forms a D loop (displacement loop) that stabilizes the t-loop [10]. A complex of six human telomere binding proteins, called shelterin, has been identified [11]. These include TRF1, TRF2, TIN2, RAP1, TPP1 and POT1. Shelterin promotes formation of a t-loop, which is critical for protecting the G-tail and maintaining telomere length and structure. WRN has also been detected in telomere complexes. It interacts with TRF2 and POT1, and regulates telomere processing during S phase [12-14]. This WRN function is biologically important, because WS fibroblasts display accelerated telomere erosion and stochastic telomere loss [15], and WS lymphoblasts show erratic telomere length dynamics [15-17]. The DNA-PK complex, which is composed of a catalytic subunit, DNA-PKcs, regulatory subunits Ku70, and Ku80, is a DNA damage sensing serine-threonine protein kinase that is critical for repair of DNA double strand breaks. This complex was found at telomeres and DNA-PKcs-deficient cells also exhibit dysfunctional telomeres [18, 19]. In addition to the similar defects of telomere in WS cells and DNA-PKcs deficient cells, DNA-PKcs interacts with and phosphorylates WRN in response to DNA double-strand breaks [20-22]. Thus, these two proteins may also cooperate in telomere metabolism.

Here, we report findings that add novel insight into the function of WRN and DNA-PKcs at telomeres. DNA-PKcs stimulates WRN helicase activity on D-loop substrates. Measurements of telomere length revealed that G-tail shortenings in DNA-PKcs-deficient cells were reversed by overexpression of WRN helicase. We propose that the DNA-PKcs and WRN cooperation play a critical and interactive role in maintaining telomere length and structure in proliferating cells.

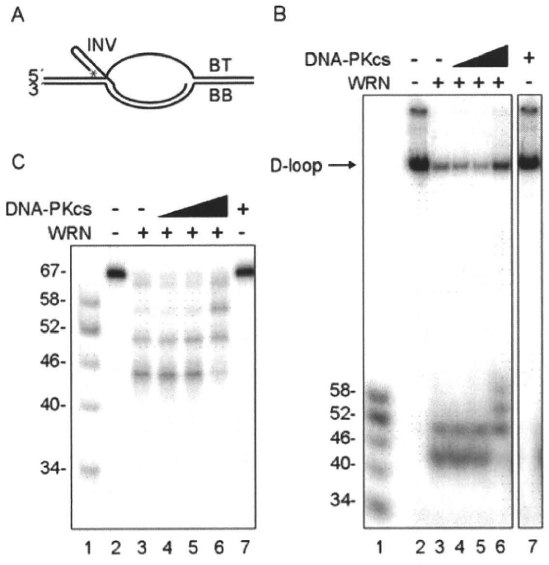

Figure 1. D-loop unwinding by WRN in the absence and presence of DNA-PKcs. (**A**) The D-loop substrate consisted with INV, BT and BB. 5'-end of INV was radiolabeled as indicated by asterisk. WRN (3.3 nM, lanes 3-6) and increasing amounts of DNA-PKcs (0.67 nM, lane 4; 3.3 nM, lanes 5 and 7; 16.7 nM, lane 6) were incubated in standard reaction buffer prior to addition of the telomeric D-loop substrate. Reaction products were analyzed by native (**B**) or denaturing gel electrophoresis (**C**). Lanes 1 in (**B**) and (**C**): A DNA ladder marker.

RESULTS

DNA-PKcs modulates WRN processing of telomeric D-loops

The effect of DNA-PKcs on WRN was analyzed using an *in vitro* telomeric D-loop unwinding assay. The DNA substrate used in this assay consists of a bubble with two 30 bp duplex arms separated by a 33 nt ssDNA "melted" region, one strand of which is annealed to an "invading" ssDNA (INV) (Figure 1A). The melted region and the invading ssDNA carry telomeric repeats, such that the DNA substrate mimics a telomeric D-loop. Previous studies with this DNA substrate showed that WRN exonuclease partially degrades and the WRN helicase unwinds and releases the INV DNA strand, which is stable after release because WRN exonuclease does not efficiently degrade ssDNA [12]. In this study, the DNA substrate was incubated with WRN in the absence or the presence of increasing amounts of DNA-PKcs. Under these conditions, WRN was not phosphorylated by the DNA-PKcs since Ku70 and Ku80 are absent. Reaction products were analyzed by native and denaturing gel electrophoresis, as shown in Figures 1B and 1C, respectively. In the absence of PKcs, WRN released 52- and 46-mer ssDNA products (Figure 1B and 1C, lanes 3), consistent with its pausing at the GGG sequence in the telomeric repeat, as reported previously [12]. In the presence of up to a 5-fold molar excess of DNA-PKcs to WRN, the ssDNA reaction products were longer, primarily 52-, 58-, and 64- nucleotides in length (Figures 1B and 1C, lanes 6). However, the total ssDNA product (and the amount of unreacted DNA substrate) was similar in WRN reactions with or without DNA-PKcs (Figures 1B and 1C, lanes 6). These results suggested two possibilities; i) the processivity of WRN exonuclease is inhibited by DNA-PKcs, or ii) the processivity of WRN helicase is stimulated by DNA-PKcs.

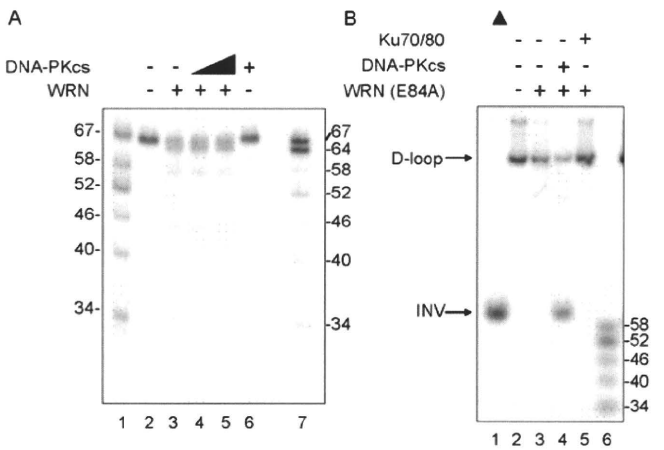

Figure 2. Differential Effect of DNA-PKcs on WRN helicase and exonuclease activities. (**A**) WRN (3.3 nM, lanes 3-5) and DNA-PKcs (3.3 nM, lane 4; 16.7 nM, lanes 5 and 6) were incubated in standard reaction buffer lacking ATP prior to addition of the D-loop substrate. Reaction products were analyzed by denaturing gel electrophoresis. Lanes 1 and 7: A DNA ladder marker. (**B**) WRN (E84A) (3.3 nM, lanes 3-5) was preincubated with either DNA-PKcs (16.7 nM, lane 4) or Ku (3.3 nM, lane 5) in standard reaction buffer prior to addition of the D-loop substrate. Reaction products were analyzed by native gel electrophoresis. Lane 1: heat-denatured D-loop substrate denoted by a filled triangle. Lane 6: A DNA ladder marker.

DNA-PKcs stimulates WRN helicase activity on telomeric D-loops

The effect of DNA-PKcs on WRN enzymatic functions was examined by incubating WRN with telomeric D-loop substrates in the absence of ATP, which inactivates WRN helicase without affecting WRN exonuclease. Under these conditions, WRN exonuclease produced 64-, 58-, 52- and 46-mer reaction products, and the distribution of reaction products was unchanged by addition of DNA-PKcs (Figure 2A). Thus, DNA-PKcs does not inhibit WRN exonuclease. The ability of DNA-PKcs to stimulate WRN helicase activity was examined by incubating an exonuclease-deficient point mutant, WRN (E84A) with telomeric D-loop substrates in the absence or presence of DNA-PKcs. WRN (E84A), which has a normal level of helicase activity but no exonuclease activity, unwinds 3.3% of the telomeric D-loop substrate in the absence of DNA-PKcs (Figure 2B, lane 3) and unwinds 66% of the substrate in the presence of DNA-PKcs, producing a full-length INV (Figure 2B, lane 4). This very significant stimulation is not observed in reactions containing Ku 70/80 (Figure 2B, lane 5), arguing against the possibility that a low level contamination of DNA-PKcs with Ku is responsible for the observed stimulation of WRN helicase. These results suggest that DNA-PKcs stimulates WRN helicase, possibly by increasing its processivity, and that this stimulation is independent of WRN exonuclease.

DNA-PKcs does not stimulate BLM helicase activity on telomeric D-loops

BLM is a human RecQ family helicase, which like WRN, is proposed to play a role at telomeres in human cells [14]. Therefore, the effect of DNA-PKcs on BLM ability to unwind telomeric D-loop DNA substrates was examined (Figure 3). In reactions containing a low concentration of BLM, BLM failed to unwind the telomeric D-loop in the absence or presence of DNA-PKcs. However, when replication protein A (RPA) was added to the same amount of BLM, BLM helicase fully unwound the telomeric D-loop, producing full-length INV, as previously reported [13]. Thus, DNA-PKcs does not stimulate BLM helicase, indicating that its interaction with WRN helicase is specific.

DNA-PKcs stimulates WRN helicase activity on non-telomeric D-loops

The ability of DNA-PKcs to stimulate WRN wild type or WRN (E84A) helicase on non-telomeric D-loop substrates was also examined (Figure 4). The results show that wild type and WRN (E84A) unwinds a small fraction of the non-telomeric D-loop substrate in the absence of DNA-PKcs, and the addition of DNA-PKcs increased the unwinding, while it enabled WRN to produce longer ssDNA products (Figure 4, lanes 9-13). Similar results were observed with telomeric D-loop DNA substrates, as observed in Figures 1B and 2B (Figure 4, lanes 2-6). These results suggest that DNA-PKcs may stimulate WRN helicase activity on D-loop structures in telomeric or non-telomeric DNA because the stimulation appears to be independent of the nucleotide sequence of the DNA substrate *in vitro*.

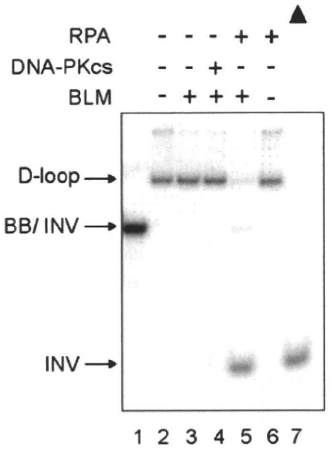

Figure 3. Differential effect of DNA-PKcs on WRN and BLM helicase activities. BLM (3.3 nM, lanes 3-5) and either DNA-PKcs (16.7 nM, lane 4) or RPA (16.7 nM, lanes 5 and 6) were incubated in standard reaction buffer prior to addition of the D-loop substrate. Lane 1: A DNA marker, [^{32}P]-INV annealed with BB. Lane 7: heat-denatured D-loop substrate denoted by a filled triangle.

DNA-PKcs does not stimulate WRN helicase on non-D-loop DNA substrates

The ability of DNA-PKcs to stimulate WRN helicase was also tested on several DNA metabolic intermediates other than D-loops (Figures 5). These included two forked duplexes with poly-T 15-mer arms, one with a 34-bp duplex region containing $(TTAGGG)_4$ and one with a 22-bp duplex region lacking telomeric repeats (Figure 5A). WRN helicase unwinds the 34-bp forked duplex in the presence of RPA (Figure 5A, lane 5), as reported previously [23]. Under the same conditions but in the presence of DNA-PKcs, WRN did not unwind this DNA substrate (Figure 5, lane 3). WRN unwinds the 22-bp forked duplex with similar efficiency in the absence or presence of DNA-PKcs or RPA (Figure 5A, lanes 8, 9 and 11). Although RPA is thought to increase

the processivity of WRN helicase, the intrinsic processivity of WRN helicase appears to be sufficient for unwinding the 22-bp forked duplex used in this experiment. Figure 5B shows that WRN and BLM helicase unwind a Holliday junction DNA substrate, and that this activity is not stimulated by DNA-PKcs. These results indicate that DNA-PKcs stimulates the processivity of WRN helicase on the D-loop substrate but not on other DNA substrates examined in this study. Because D-loops may be enriched in telomeric regions *in vivo*, this is consistent with the proposed roles of WRN and DNA-PK specifically in telomere length maintenance.

Telomeric DNA can exist in a closed D-loop form or an open form, with the open form more likely to occur during DNA replication or in response to DNA damage. Therefore, the ability of DNA-PKcs to stimulate WRN helicase was also tested on a telomeric DNA substrate that resembles the telomere in an open conformation (Figure 5C). For this purpose, a DNA substrate was prepared containing a telomeric duplex DNA upstream of G-tail [24]. Note that the polarity of WRN helicase is 3'-5', allowing it to unwind duplexes with a G-tail, but not duplexes with a 5'-ssDNA tail. The DNA substrate used in these experiments includes both a G-tailed duplex as depicted in Figure 5C and a second species, which is likely to be a bi-molecular G-quadruplex structure formed by annealing of the ssDNA tails of two G-tailed duplexes. The latter structure has a slower electrophoretic mobility than the G-tailed duplex (Figure 5C, lane 1), and it is destabilized by WRN (Figure 5C, lanes 2–5) or boiling (Figure 5C, lane 6).

WRN exonuclease degrades the open telomeric DNA substrate starting at the 3'-OH blunt end, and WRN helicase unwinds and releases the shortened strand from the G-tailed duplex (Figure 5C, lane 2). DNA-PKcs did not stimulate WRN helicase on this DNA substrate (Figure 5C, lanes 2-5). The results suggest that DNA-PKcs stimulates WRN helicase on a telomeric D-loop substrate, but not on a G-tailed DNA duplex, an open form of a telomeric D-loop.

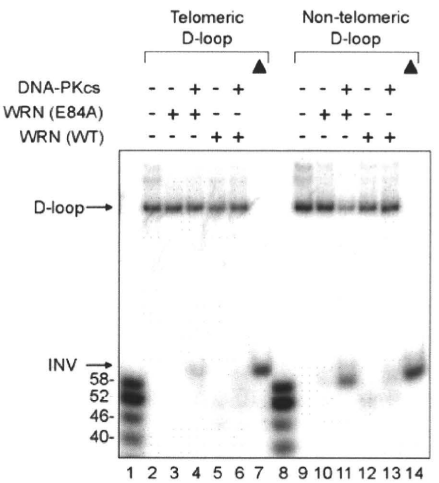

Figure 4. Effect of DNA-PKcs on WRN helicase activity on telomeric and non-telomeric D-loops. WRN wild type (WT) (3.3 nM, lanes 5, 6, 12, and 13) or WRN (E84A) (3.3 nM, lanes 3, 4, 10, and 11) was preincubated with DNA-PKcs (16.7 nM, lanes 4, 6, 11, and 13). A telomeric (lanes 2-6) or a non-telomeric D-loop substrate (lanes 9-13) was added to the reaction. Lanes 1 and 8: A DNA ladder marker. Lanes 7 and 14: heat-denatured telomeric and non-telomeric D-loop substrates, respectively, denoted by filled triangles

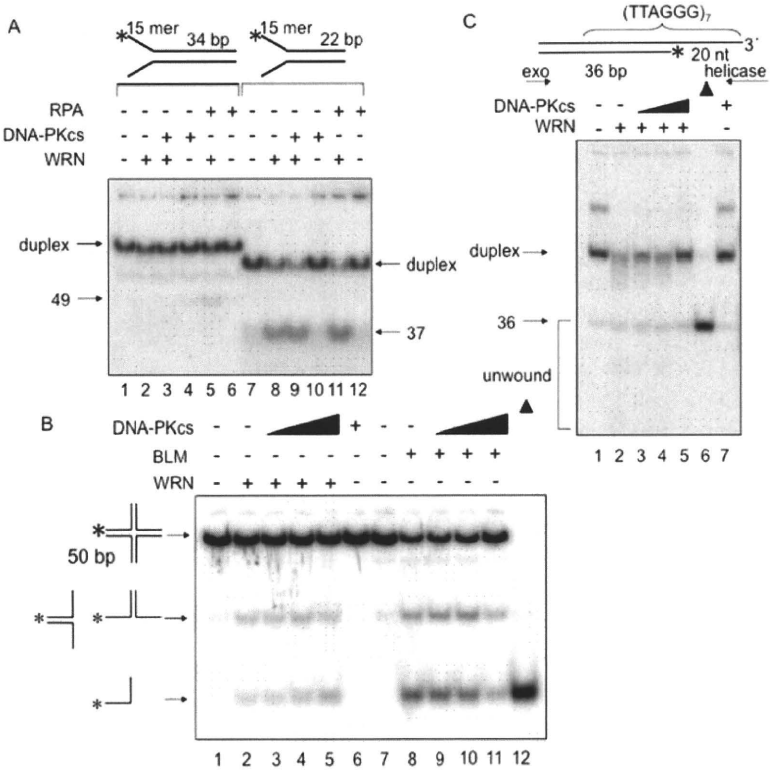

Figure 5. DNA-PKcs fails to alter WRN helicase activity on forked duplex, Holliday junction and G-tailed telomeric DNA substrates. DNA helicase assays were carried out in the presence of the indicated proteins and DNA substrates. (**A**) WRN (1 nM, lanes 2, 3, 5, 8, 9, and 11) and either DNA-PKcs (5 nM, lanes 3, 4, 9, and 10) or RPA (5 nM, lanes 5, 6, 11, and 12) were incubated in standard reaction buffer prior to addition of a 34 bp forked duplex (0.5 nM, lanes 1-6) or a 22 bp forked duplex (0.5 nM, lanes 7-12). (**B**) WRN (4 nM, lanes 2-5) or BLM (2.5 nM, lanes 8-11), and DNA-PKcs (4 nM, lane 3; 8 nM, lane 4; 20 nM, lanes 5; 2.5 nM, lane 9; 5 nM, lane 10; 12.5 nM, lane 11) were incubated with in HJ reaction buffer prior to addition of Holliday junction (0.5 nM, lanes 1-11). Lane 6: DNA-PKcs (20 nM) alone. Lane 12: heat-denatured Holliday junction denoted with filled triangles. (**C**) G-tailed duplex (0.5 nM, lanes 1-5 and 7) was incubated with WRN (7.5 nM, lane 2-5) and DNA-PKcs (6.25 nM, lane 3; 12.5 nM, lane 4; 25 nM, lanes 5 and 7) in standard reaction buffer. Lane 6: heat-denatured G-tailed duplex denoted by a filled triangle.

Protection of G- tail by WRN helicase activity

The above studies suggest that DNA-PKcs stimulates telomere unwinding by WRN *in vitro*, but do not address whether this interaction is important *in vivo*. Nevertheless, previous studies are consistent with this possibility. In particular, telomere length decreases more quickly in Terc$^{-/-}$/DNA-PKcs$^{-/-}$ mice than in Terc$^{-/-}$ mice [25], and Terc$^{-/-}$/WRN$^{-/-}$ but not WRN$^{-/-}$ mice have a telomere dysfunction [26]. Thus, experiments were performed to test whether the interaction between WRN and DNA-PKcs is important for telomere length maintenance *in vivo* (Figure 6). For this purpose, a G-tail telomere hybridization protection assay (HPA) was performed with DNA purified from U-2 OS cells, which are telomerase negative. The G-tail telomere HPA assay, shown schematically in Figure 6A, accurately measures telomere G-tail length. The G-tail telomere HPA assay was first performed using U-2 OS cells which stably express an shRNA targeted to WRN or control U-2 OS cells which stably express a scrambled shRNA with no significant homology to known human genes (Figure 6B). The results show that G-tail length is significantly shorter in WRN knockdown cells. The effect of DNA-PKcs on the G-tail length was examined using the cells transfected with an siRNA targeted to DNA-PKcs (Figure 6C). G-tail length was also slightly shorter in DNA-PKcs knockdown cells, compared to

cells transfected with control siRNA. Overexpression of N-terminally EYFP-tagged WRN (E84A), an exonuclease dead mutant, in the DNA-PKcs knockdown cells reversed the G-tail shortening. This suggests that endogenous WRN exonuclease is responsible for a part of this outcome of the shortening in the absence of DNA-PKcs, and an excess amount of WRN (E84A) prevents the exonuclease from attacking the G-tail and exhibit unwinding activity. However, a similar result was obtained by overexpression of N-terminally EYFP-tagged WRN wild type in the DNA-PKcs knock down cells. There may be a mechanism to support an access of an exonuclease domain of WRN (E84A) but not WRN wild type to the G-tail in cells (Figure 6C), because the domain (1-239 amino acids) is important to regulate its binding to forked duplex, which is resemble a part of D-loop substrate [27].

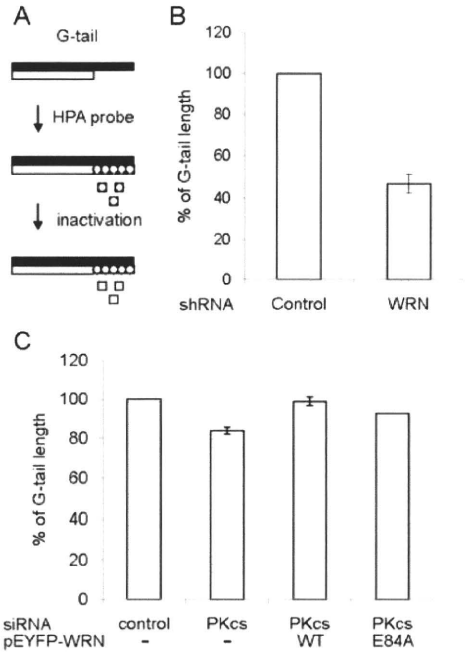

Figure 6.Quantification of telomere G-tail length by hybridization protection assay in DNA-PKcs knockdown U-2 OS cells. (**A**) A schematic of the HPA for telomere G-tail. Non-denatured genomic DNA was incubated with acridinium ester (AE)-labeled 29-mer telomere HPA probe. The AE of unhybridized and mis-hybridized probes was hydrolyzed, and chemilumines-cence from AE of hybridized probes was measured. (**B** and **C**) G-tail length of cells expressing an shRNA control or an shRNA against WRN was examined in panel B. G-tail length of cells transfected with siRNA against control (left), siRNA against DNA-PKcs (middle left), siRNA against DNA-PKcs with pEYFP-WRN (middle right), or siRNA against DNA-PKcs with pEYFP-WRN (E84A) (right) was examined in panel C. The G-tail length in the control cells was represented as 100%. Data are represented as mean +/- standard errors of two independent experiments.

DISCUSSION

This study demonstrates that DNA-PKcs stimulates the apparent processivity of WRN helicase but not WRN exonuclease on telomeric and non-telomeric D-loop substrates *in vitro* and that overexpression of WRN helicase reverses telomere G-tail shortening *in vivo* caused by knockdown of DNA-PKcs in U-2 OS cells. Based on these results, we propose a model for the role of WRN and DNA-PKcs in D-loop unwinding (Figure 7). The key points of the model are as follows: 1) In the absence of DNA-PKcs and WRN exonuclease, WRN helicase dissociates from DNA prior to release of a full-length invading strand, resulting in reannealing of the unwound region; 2) when WRN exonuclease degrades the 3' tail of the invading strand, WRN helicase releases the shortened invading strand, even in the absence of DNA-PKcs; 3) DNA-PKcs stimulates WRN processivity, so that exonuclease-deficient WRN or WRN is able to release an intact or nearly intact invading strand from the D-loop, respectively. This mechanism would protect telomeric DNA 3'-ends, prevent telomere shortening, and potentially avoid p53-p21-dependent replicative senescence.

The results also indicate that DNA-PKcs stimulates WRN-catalyzed unwinding of non-telomeric D-loop, implying that WRN and DNA-PKcs could cooperate to unwind recombination-associated D-loops in genomic regions other than the telomere. This is consistent with a possible role of WRN in processing D-loop intermediates in homologous recombination, which is supported by several *in vitro* studies [8, 28].

Previous studies also show that POT1 and RPA, WRN and BLM interacting proteins, stimulate WRN and BLM-catalyzed unwinding of telomeric D-loop substrates *in vitro* [13]. However, the mechanism(s) of this stimulation may differ from the mechanism by which DNA-PKcs stimulates WRN helicase. POT1 and RPA are ssDNA binding proteins. They stabilize ssDNA and prevent ssDNA reannealing, rather than preventing WRN dissociation from the substrate through their interaction with WRN. Unlike POT1 and RPA, DNA-PKcs has a low affinity for ssDNA, but high affinity for junctions between ssDNA and dsDNA [29]. Thus, DNA-PKcs might bind to the ssDNA/dsDNA junctions of D-loops that have been partially melted by WRN and prevent ssDNA reannealing. Direct interaction between WRN and DNA-PKcs was demonstrated [21]. It is also possible that DNA-PKcs prevents WRN from dissociating from the DNA substrate, and that this interaction stimulates the processivity of WRN helicase. Recently, it was reported that deacetylation of histone H3 lysine 9 by